

## Response to the reviews of the manuscript:

### *Geodetic mass balance record with rigorous uncertainty estimates deduced from aerial photographs and LiDAR data. Case study from Drangajökull ice cap, NW-Iceland*

By E. Magnússon, J. M. C. Belart, F. Pálsson, H. Ágústsson and P. Crochet.

We have done two main changes of the manuscript from the published TCD paper. Both have resulted in substantial shortening of a relatively long paper. These are:

- i)** As pointed out by referee #2 (Christopher Nuth) the simple mass balance model presented in Fig. 10 was a bit out of place given the rest of the paper. It has therefore been omitted as well as everything related to it, including the results of the mass balance model on decadal timescales, which was presented in Fig. 9. In addition to these changes on Fig. 9 the results from east and west section of Drangajökull has been combined into single panel and panel **b** from Fig. 10 has been added as the third panel. Panel **c** in Fig. 10 has been replaced by references in new manuscript.
  
- ii)** In the new manuscript we do not scale the positive degree day factor (*ddf*) using the sum of positive summer temperatures (using daily temperature grids), winter precipitation grids and the measured volume change. This change of the manuscript is the outcome of an attempt to use both identical temperature grids and identical precipitation grids for the whole time span of the study. At the time of submission the 1kmx1km daily temperature grids (Crochet and Jóhannesson, 2011) were not available for the year 2011. This resulted in two different *ddf* scaling estimations, one for the period 1960-2005 and another for the period 2005-2011 using different sources of temperature grids. Since the submission, the former temperature dataset has been extended, hence a single scaling for the period 1960-2011 could be carried out. We also used two types of daily precipitation grids, but the record which we referred to as  $p_2$  in the TCD paper has been extend back in time now available for the whole period 1960-2011. The simple model that we obtained using the *ddf* scaled using both identical temperature and precipitation maps for the whole periods, resulted in worse fit on decadal timescales than shown in Fig. 9 in the TCD paper. This further supported our decision to omit the model in the current manuscript; an attempt to explain why this resulted in worse fit is beyond the scope of this paper. This also led to the decision to omit our attempt to estimate the *ddf* scaling and use instead the range of reported *ddf* values, using comparable temperature data for Langjökull, Hofsjökull and Vatnajökull ice caps in Iceland, to constrain a *ddf* value with uncertainty. The result of these changes is somewhat different seasonal volume correction and uncertainty, leading to slightly changed values of mass balance rates in the new version of the paper.

In addition to these two main changes we have made numerous smaller changes mostly as reactions to the comments made by the referees. Below we list the comments made by the referees and our response, which states the consequent changes, often including further explanation. In the few cases where we have not done any changes we explain why.

## **Anonymous Referee #1**

### **General comments:**

*I'm uncomfortable with the way the authors brush over the use of lidar as control for a photogrammetric DEM and I think they could provide better acknowledgement to papers that have used this approach (which I point out in the specific comments below).*

It was not our intention to brush over the use of LiDAR as control for photogrammetric DEMs, and therefore included a reference to Barrand et al. (2009) in the previously submitted version. We however realize that a reference to James et al. (2006) is a more appropriate reference and therefore included it in the current version as first reference to such work and at few locations in the current manuscript where it is appropriate.

*First, as the underlying lidar DEM is of paramount importance to the quality of the DEMs, it is surprising that very little is said about the lidar data set itself. This is addressed in another publication and the authors provide a blanket accuracy statistic of 0.5 m. However, these sorts of figures are typically associated with actual lidar hits (not interpolated) over a reflective surface (which wet glaciers and dark mountain rocks typically are not). The DEM used by the authors is interpolated to a 2 x 2 m grid (no info on the original resolution) which will degrade quality further and contribute error to the resultant ground control.*

We added info on the specifications of the Lidar instrument and data (including average density of the LiDAR point cloud) as well referencing more clearly where further info can be found. We also explain further the validation of the Lidar data that we give a reference to (Jóhannesson et al., 2011). However as mentioned in the manuscript, errors in the LiDAR data are inherent in the errors estimates of the photogrammetric DEMs. Consequently, random errors in the photogrammetric DEMs are likely to be slightly overestimated. Bias error in the LiDAR DEM should however be cancelled out since all elevation changes are effectively carried out in the elevation reference frame of the LiDAR DEM.

*There is also significant uncertainty associated with identifying homologous points between an optical image and a shaded-relief topographic model. I think more discussion about the lidar DEM and the resulting errors are required. At the very least acknowledgement that a significant component of the errors they report could be as a result of poor quality GCP. Second, typical photogrammetric adjustment algorithms expect ground control to be an order of magnitude*

*higher accuracy than the resulting DEM elevations and the sigma values that control the degree to which these parameters can be adjusted in the block adjustment are set accordingly. In order to use atypical quality ground control, especially when providing a time series of surfaces which are to be compared, it is important to address how the system deals with the higher error in the GCPs. Changing the sigma values for the adjustment can have a significant impact on the RMS errors of the GCP which the authors have provided in Table 2 but without appropriate values for sigma, the RMS errors are not good indicators of data quality. I appreciate that all this is detail that may not be of great interest in an already long manuscript but there needs to be an appreciation that it is not as straightforward as the authors imply, especially when they suggest in the conclusions that satellite imagery can be used in the same way.*

In the current version we have added info on the assigned uncertainty (as standard deviation, sigma) of GCPs both vertical and horizontal, and a statement that this is potential source of some part of the derived errors. Despite potential problems with the GCPs from the LiDAR DEM, the validation of the photogrammetric DEMs reveals in our opinion rather satisfying result. Regarding the replacement of Lidar with high resolution satellite data, this is already in use in geodetic mass balance studies i.e. (Papasodoro et al., 2015).

*The methodology could be written in a way that's easier to follow. Several methodological issues are raised in a number of locations in Sec 2 which would be easier for the reader if they were addressed together. Specifically, the GCPs and placement strategies, the manual editing and delineating glacier margins. It's also unclear to me how the conversion of glacier volume changes to w.e. is addressed or if in fact it has. The correction for date offsets in DEMs has been addressed (or purposely ignored) in a number of recent publications but the paragraph that discusses this issue is lacking literature support.*

Some of the text related to the GCP placement strategy has been moved to fulfill this. We do not find a better place for the text regarding the manual editing, than including it as part of the description on how the photogrammetric point clouds are subsampled and revised. We understand the point made regarding the location of the text on how we delineate the glacier margin. Most of this text does however not deal with the orthorectified photographs, hence it would be a bit of out of place if this was added e.g. to the end of section 2.2 right after the method description regarding the orthophotographs. We therefore think it is better to have this in a separate section. It is clearly stated in the manuscript that we are applying conversion factor including associated uncertainty from Huss (2013) to convert from volume to mass change. This study does not intend to add anything to the much appreciated study by Huss on this conversion factor and the related uncertainty.

*The correction for date offsets in DEMs has been addressed (or purposely ignored) in a number of recent publications but the paragraph that discusses this issue is lacking literature support.*

It was not our intention to claim this as something new and we realize that this lack of references was awkward. In the current version we have added references where application of various kind of date correction is investigated.

*The conclusions could be strengthened. The first paragraph is awkward and isn't describing anything new; several previous papers have generated DEMs at various epochs without support from field data. The second paragraph describes the contribution from this manuscript but does not make sufficiently clear its significance. The revelation of the importance of seasonal corrections is also not that surprising especially for glaciers with high annual turnover. This case could be made stronger with more reference to previous literature that deals with this earlier in the manuscript. Finally, the resultant estimates for B I G would be more meaningful with context.*

In our mind the message of the first paragraph is really one of the most important message of this paper. We can improve the methods in geodetic mass balance studies and high resolution DEMs from the present are the key data to do so. We therefore list in the current conclusion the usage of the LiDAR DEM in this study. Even though some studies have used high resolution DEMs for part of the work flow described here, we are not aware of any that have used the potential of such data to the same degree as we do in this study. The use of high resolution DEMs derived from satellite sensors such as Worldview or Pléiades as full replacement of Lidar DEM for all part of the work flow is yet to be attempted, but we find it likely that such studies will be successful.

In the second paragraph we have added a sentence to further clarify the significance of the error analysis carried out and the comparison with other uncertainty estimates. We do agree that the importance of seasonal correction for glacier with high mass turnover is maybe not very surprising for many readers. We however find the geodetic mass balance record presented here such a good example as a reminder that great care should be taken when interpreting geodetic mass balance records, that have not been date corrected. Finally we have added a couple of sentences to set the mass balance records of Drangajökull into perspective with other records from Icelandic glaciers.

#### **Minor comments:**

*Page 4734*

*Line 2 – is 'constraints' the right word here? Maybe, “: : : can be used to control glacier surface DEMs: : :” or simply “: : :can be used to extract glacier surface DEMs: : :”*

Changed according to the latter suggestion.

P4735

L14 – the sea-level

Corrected

*P4738 L8-15 – While the lidar data collection of Drangajökull is covered elsewhere, it would be useful to the reader to include some basic information here since the lidar underpins the rest of the data in this manuscript. Who undertook the survey and instrument used and basic flight parameters I would have found useful. When reading, I assumed this was a data set with which I was familiar but realised after consulting Johannesson et al. (2011) that it was not.*

Added basic information of the instrument (the model of scanner and a reference for more technical details). Also added more information on how the point cloud was interpolated as a grid with 2m x 2m cell size.

L19 – manual editing not edition

Corrected

*L26-27 – Was a similar set of ground control points used in each model? I think the authors explain this on P4739 L3-5 where Kraus (2007) is cited but the language isn't clear here. The meaning of 'regular scheme of distribution' isn't clear. Maybe state this more explicitly. Later in the manuscript you suggest that they were positioned to be spread around the glacier and throughout the vertical extent of the terrain. I think this is important and should be stated clearly. The whole methodology described here was first presented in James et al. (2006) (and again in James et al., 2012) and are a more appropriate and accessible reference than Kraus (2007).*

The locations of GCPs is shown in Fig.2, which is highlighted further in the revised version of paper. The sentence regarding 'regular scheme of distribution' has been rephrased. We also state now that the vertical span is covered by the GCPs. We added a reference to James et al. (2006) and state that we are following a similar approach. We however still include the reference to Kraus (2007) as a textbook in photogrammetry since the distribution of GCPs is something which applies to photogrammetry in general.

P4739

*L1-3 - This one sentence implies that extracting GCP from lidar is trivial but I do not think this is true and certainly becomes less trivial with satellite imagery as raised in the conclusions.*

We have added info on the assigned uncertainty of GCPs, both vertical and horizontal, and a statement that this is a potential source of some part of the derived errors. We disagree regarding

the difficulties of using satellite imagery and DEMs for extracting GCPs. If orthorectified images are available from the high resolution data it should be easier to identify and locate common points in aerial photographs and the satellite data compared to using hillshade images.

*L1-5 – Again, I think an acknowledgement to the work in James et al (2006) is appropriate, predates Kraus (2007) and is more accessible to readers.*

See reply to comment above

*L19-21 – I think I know what you mean here but the sentence is awkward and I don't think this will be clear to many readers. Can you be clearer about what you mean by matching in lower resolution? I presume you mean using a reduced resolution image to undertake the matching which typically improves matching success in low contrast areas but I don't think most readers will know this. Also, the effect of a larger window size and lower correlation coefficient will be useful for readers not familiar with stereomatching.*

This has been rephrased for clarification.

*L25 – why the different grid resolutions? This does not coincide with GSD from Table 1.*

Explained in the current version of the manuscript.

*P4740*

*L6 – again why the two different grid resolutions here?*

See next comment above.

*L7-9 – Where/why is their only monoscopic imagery? Your text and Figure 2 suggests that all your imagery is stereoscopic. Also, for the older epochs, the elevation of the lidar will be quite different at the contemporary ice margin and will result in fairly significant errors in the orthoimages especially if off-nadir parts of the imagery are used in orthorectification. For this reason I think you can't use the blanket term "accurately" on L8. For delineating the margins maybe this error isn't that important but you can't say that it's accurate. Maybe specify estimate worst case scenario errors and state this is sufficient for delineating ice margins.*

This is explained in more details in the current version, including justification on why we can use the LiDAR. We however deleted the word "accurately".

*L19-21 – I think this is a very important point as is true for comparisons between the other DEMs as well.*

We agree.

*L23 – deduced is not the right word. Perhaps derived?*

Corrected accordingly

*Fig S1 – Can you specify in this figure that the white areas are those that required interpolation?*

Text in caption for Fig. S1 changed in such way that it is clear that white areas on glacier are interpolated with kriging using the point cloud locations and the difference between the point cloud and the Lidar DEM. The numbered areas however interpolated in different manner explained in the main text and in the Supplement [supplement not yet changed].

*P4741*

*L2-3 – this is a very complicated way to say that only bare surfaces were used in the quality assessment. It would be more straightforward to say this explicitly and then add the 40 horizontal distance condition.*

Rephrased to clarify.

*L4 – semiautomatic classification is vague. Supervised classification?*

Due variable brightness in the scanned old aerial photographs it was difficult to apply fully automatic classification of snow covered areas. Hence the results from such automatic classification had to be reviewed and redone locally for some areas using different thresholds. Hence the word semiautomatic. Supervised classification is commonly referred to as a method in image classification, which we are not applying.

*L24-27 – this sentence is awkward*

Sentence has been restructured.

*P4742*

*L25 – of the errors*

An 's' added to error.

P4743

*L1-4 – this really should be raised earlier when GCPs are first raised.*

This is mentioned there as well in the current version of the paper and part of the text has been moved. We however think it is worth mentioning this again here in relation to the semivariograms, which had not been explained in Sect. 2.1

*L6 – ‘allow’ rather than ‘secure’*

Changed accordingly.

P4744

*L1-2 – another bit that should be realized earlier since this is not part of the bias correction discussed here.*

This is also mentioned earlier.

P4746

*L1-2 – do you mean they are less dense inherently as part of the DEM generation process or by your design because I find the opposite to be true. The snow free ice surface has quite a lot of texture.*

This is true. We therefore changed the classification in the text to snow covered versus bare ice or ground, to be more precise about the density. Reference to the Supplement was also added to make this clearer.

*L8-10 – this should reference Cox and March (2004) which is the first instance I know of that points out the variability of elevation changes will be lower than absolute elevation.*

Citation added.

*L16 – photogrammetric not photographic*

Corrected

P4749

Sec 2.6 – lacking literature support here for a very common problem.

Citation of few papers added.

P4757

*Sec 3.3 – how were the w.e. units derived? It's typical to address the snow/firn/ice density issue here.*

As stated in the Sect. 2.7 we use conversion factor with uncertainty from Huss (2013).

P4759

*L24-2 – The interpolation of surface change rather than surface elevation due to its lower variability is not new. For example, Cox et al. (2004) uses this approach in their comparison of geodetic and glaciological mass balance techniques. This should be acknowledged here and where this was raised in the methodology.*

Citation to Cox and March (2004) added.

P4760

*L3-13 – As I have said in my general comments above, there's an important element to using relatively low-quality ground control to control a photogrammetric model that has been omitted from this manuscript.*

In the current version more info is included on the how the GCPs are used in the DEM processing. We also give reference, both here and in introduction to a study where Pléiades data is used as replacement for the LIDAR to collect GCPs.

P4764

L25-26 - the first sentence here is awkward. Consider revising.

See reply to general comment.

P4765

*L4 – DEMs*

Corrected

*Figures – I find the figures to be too small in print format. The annotation text is almost invisible.*

We do agree. Figures 5, 7-9 are supposed to be single column figures the rest was intended as full 2 column figure, which should take care of this problem.

*Figure 1 could be improved by making part c the main figure with two insets. The location of Vatnajökull and Langjökull are not relevant here.*

We find the figure better arranged like this. The letters L and V have now been deleted.

*Figure 2, each subfigure could be a full figure with the relevant DEM as the background image maybe to appear later in the paper. This would be more useful to readers.*

The background image here is in all cases the Lidar DEM. The purpose of this image is to show the distribution GCPs and the coverage of the aerial photograph for each epoch. The coverage of the resulting DEMs are shown in Figure 3 as difference compared to compared to LiDAR off ice, and as hillshade image on ice.

*Figure 3 is completely illegible in this size. Should 'vicinity of the glacier' be 'off ice'?*

We agree, therefore this is intended as full 2 column figure in the final version of the paper. Caption changed according to suggestion.

## **Referee #2 (Christopher Nuth)**

### **General comments:**

*The manuscript is rather long and at some points a little difficult to follow from all the details. I can understand that it was not easy to get all the specific details into a logical framework, but I think this may need some re-consideration to determine which information is important to keep, and which may be thrown away. In addition, the application of the entire mass balance model through the entire time series (Fig 10) is highly interesting, but may rather be suitable for a separate publication. There is not enough space in this manuscript to discuss these results, and why the mass balance model may or may not fit to the geodetic mass balance measurements. I think it is fine to use the mass balance model to estimate your seasonal corrections, but consider leaving it at that.*

The work on the seasonal correction has been simplified (see initial comments by authors above) and consequently the text related to it has both been removed or changed. We agree that the mass balance model was bit out of place in this paper hence, everything related to it has been removed from the current version of the paper.

*In terms of the error analysis and description, there are a number of points that need clarification and consideration. First, I think there is an important reference missing: Zemp et al. 2013 <http://www.the-cryosphere.net/7/1227/2013/>.*

This reference both was and is now included in the manuscript.

*There needs to be a clear separation between the types of errors one is discussing, in particular the difference between bias and random errors (accuracy and precision). As far as I know, Rolstad et al. (2009) quantified the influence of the random error component over the glacier area at question. I am not sure whether your simulations are for the total error, including both systematic and random components but I believe you have modelled a potential systematic error over the glacier, and then correct for it? If this is the case, then the two studies may not be as easily comparable, but certainly should be discussed.*

In this paper we estimate with geostatistical approach both bias correction and the uncertainty of it caused by random errors in the DEMs. This is thoroughly explained in the manuscript. Rolstad et al. (2009) applies higher order correction on the DEM difference and the uncertainty in the derived volume change represented as range of likely bias error (one sigma). The latter value in both methods is therefore comparable. We however point out in our discussion that the strength of our method is that it estimates bias and its uncertainty based on the same derived probability distribution, as the mean of the probability curve and 95% confidence interval. Other bias correction or higher order corrections, including the one by Rolstad et al. (2009) lack clear connection with the probabilistic mean bias, which may result in reasonable width of uncertainty but centred around an inaccurate value.

*Furthermore, more detailed description of “Nscore”ing needs to be made. It is ok to reference to others, but it will allow the reader to understand more directly what you are doing. I am particularly curious about the influence of transforming the data into a normal distribution for calculating the errors, and then whether this assumption then allows for more realistic, representative error estimates for DEM differencing, or if alternatively, provides unnecessarily small error estimates since the inherent error distributions are not normally distributed. I think discussion around this assumption should become a more significant part of this manuscript, and certainly may still be open for discussion.*

We have rewritten the text describing this step, including explanations why this is done. This step is simple something which enables the usage of SGSim without the variable being normally distributed. In our case the distribution of the error data was generally close to resemble normal distribution, but it is sometimes a bit skewed (particularly in 1946, see Fig. 3). This step, which Statios, the copyright owner of WinGSlib, mandates as the first step before carrying out SGSim ([www.statios.com/Training/index.html](http://www.statios.com/Training/index.html)), basically takes a variable and transforms it into a variable with histogram fitting normal distribution with zeros mean and  $\sigma=1$ . It is not just a simple shift and multiplication of the variable. It also carries out local stretching of the variable in order obtain good fit with normally distributed histogram. We have not checked the WinGSlib code to see exactly how the nscore function operates but if someone plans to carry out the error analysis explained in this paper without using WinGSlib, writing a code that

achieves what nscores does is not difficult and we can think of several ways to do that, but this not the right place for such explanations.

**Minor remarks:**

*Pg4738 L13: "The Lidar DEM..."*

Changed accordingly.

L19: "manual editing of the"

Corrected.

*Pg4739 L7- Which year was the monoscopic coverage?*

*L8 – I don't understand how you can use a modern DEM to orthorectify a historic imagery and actually reveal accurately front positions? Since the front of the glacier is where the most change is happening, here is where one would expect the worst results from orthoprojection of a historic image on a modern DEM...*

See reply to referee #1 on similar comment.

*Pg4740 L26-27 – So here, you are extracting a 2x2m elevation at a sampling distance of 20m. This inherently causes resolution problems for your comparisons related to roughness, curvature and ultimately resolution. To be completely precise, one should average the LIDAR with a 10x10 pixel window around each 20m grid sampling...*

This is misunderstanding. Part of this paragraph has been rewritten according to suggestions of reviewer 1, so hopefully it is clearer in the current version. We don't resample the LiDAR DEM into 20mx20 grid. Instead, for each point of a photogrammetric point cloud under inspection, we obtain a value of difference compared to the 2x2m LiDAR. These difference values are interpolated in a 20x20 grid, creating thus the elevation difference map.

*Pg4741 L21: I agree that it may be highly unlikely, but it is very easy to test by making a scatterplot of [elevation difference divided by slope tangent] by [aspect] ...*

We did check for the 1975 and 1946 DEMs what horizontal shift relative to the LiDAR DEM would minimize the standard deviation of the vertical elevation difference (Berthier et al., 2007) in ice and snow free areas. The check for 1975 resulted in 0.5 m shift, which we considered insignificant. When doing this for the 1946 DEM the unglaciated DEM resulted in 5.7 m shift

in west but 0.0 m north, which was a bit puzzling. We however would not consider such shift a big problem, since it would generally only lead vertical errors of few tens of cm (given rather gentle slopes of the glacier), and hardly cause bias exceeding more 10 cm, which is small compared to the uncertainty of the 1946 bias correction (1.66 m). We however decided to redo the test using only data within 3 km from the glacier margin. This resulted in quite different values with 4.7 m shift west and 5.0 m north. When cutting the DEM into 4 quarters we get variable results with shifts varying between 8 m west to 9 m east and 12 m north to 12 m south. Our conclusion from this was, that when the vertical errors are as large as in the 1946 DEM, this method can only discriminate between actual vertical errors and real horizontal shift on length scales which are larger than RMSE of the GCPs (3 m for 1946). The uneven distribution of data, the location of the largest vertical errors and how it matches with the slope and aspect of the DEM is likely to result in artificial horizontal shift on the order of several meters. We therefore don't see reason to override the horizontal constrain of the GCPs with results from such test. We now however state that it is 'unlikely' instead of 'very unlikely' the horizontal shift exceeds the horizontal RMSE of the GCPs.

*P4742 L7: This step needs to be explained in more detail. How does the transform affect the data, what kind of transform is it... It would also be beneficial to defend this choice or provide a background on why you chose this direction.*

See answer to general comment above.

*L11: "...nscored input data, in which the semivariogram..."*

Changed accordingly.

*P4743 L15-20: I don't follow the argumentation about the 1946 DEM. According to Fig 4c, I see that the range for low contrast surfaces is closer to 1600 m, but this for changes between 1946 and the LIDAR. In either way, this argumentation needs to be spelled out a bit clearer for the reader.*

This text has been rewritten and extended to explain better the argumentation. The range of semivariogram for the difference between LiDAR and the 1946 data from the low contrast areas has no real meaning because it is controlled by the elevation changes not the errors. The only significance of this plot for error analysis is, as explained in the current version of the manuscript, for short distances.

*L24-28: Fine to filter by slope but I imagine there is more a problem about resolution between your reference and slave DEMs, and thus curvature and roughness will have a large impact, since you compare a 2m point elevation to a 20m pixel elevation.*

See answer to previous comment regarding the pixel size of the LiDAR and interpolation of the difference between the photogrammetric point cloud and the LiDAR.

*P4744 L6: a 500 by 500 m window is rather large and a bit excessive. This creates unnaturally smoothed values. Why not use 100 by 100 m since you end up sampling at this distance in the end (L26)??*

We are applying the 500x500 median filter on the difference grid (interpolated difference between photogrammetric point cloud and 2x2m LiDAR DEM) to obtain a comparison value with the unfiltered difference grid. If the difference between median filtered and the unfiltered value exceeds certain limit ( $2\sigma$  of the difference grid after masking glacier or snow covered areas and high slope area) it is considered an outlier. If such outlier removal is carried out with too small median filter the median value at each location is calculated from too few samples (25 or less for 100x100m filter). The outcome median value becomes much more random than it should, resulting in many good points being classified with this approach as outliers and many outliers classified as good points.

*P4745 L16-20: Could the spatially varying mean error really be used for correction? It is only produced from a simulation, and not really based on any truth over the glacier. What strikes me is the trend (in Fig 4d) from lower glacier to upper glacier, this type of bias adjustment, if not certain, would change the data significantly, and probably also the interpretation. Also, in the end, what is the value of the mean of the derived probability function? And where is this derived, only over the glacier, or over the entire sample?*

For obtaining volume changes it makes no difference whether you subtract the spatially varying mean (mean value for 1000 simulation at given cell) or subtract the mean over the 1000 spatial mean values calculated over the glacier surface for each simulation. The corresponding volume of the corrections is the same.

It is true that the simulation are not based on truth over the glacier but this is generally also the case for all bias and even more so higher order correction applied in geodetic mass balance studies. If asked for individual cases: Which correction is closer to the true error, a bias correction obtained using the mean error outside the glacier or bias correction obtained with the approach explained in this paper? The answer is we don't know. The key difference is however that the latter is based on estimated probability distribution, whereas the former is just a single value without any knowledge on the likelihood of this correction being close to the average error. We argue that applying geo-statistical simulations to obtain simultaneously bias correction and uncertainty estimate is better approach than applying zero order or higher order correction using the data outside without any connection to statistic and therefore without being

able to say if the correction applied corresponds to the probabilistic mean of an average DEM error within the glacier.

The trends seen in Fig. 4d are controlled by the input into the SGSim, the spherical variogram model and the DEM error data outside the glacier. Data near the glacier margin and at the nunataks has naturally far more effect on the observed trends than data much further away from the glacier. Therefore if you obtain 4 m error at the glacier margin, it can be argued that it is more likely that the error on the glacier nearby is 4 m rather than 0 m, particularly when you have a semivariogram indicating high correlation in the error between the points over the given distance. This also explains why the obtained mean value Fig. 4d far from any error data is of relatively small magnitude.

As stated in the manuscripts the value of the mean of the derived probability function is given as the value  $z\_bias$  in Table 2. If this question regards the significance of this term we refer to the explanation above. To clarify further we modified the caption of Fig. 4 in such way that it should be clear that we are calculating the mean of the derived probability function used for bias correction for the glaciated part of the DEM. This is also clearly stated in the main text.

*L24-27: It is still not clear what the difference to Rolstad et. al. (2009) is? As far as I see it, is the transform to normal distribution is different, but it doesn't seem like the range changes so much (between fig 4a and b). Can you clarify more specifically why there is a difference, and what that difference is.*

In this paper we explain thoroughly our approach, resulting in rather long paper. We also explain how Rolstad et al. (2009) obtain their uncertainty; hence the difference between the methods should be clear. The main difference is not the nscoring of the data, which is just a required step for successful SGSim. The nscoring has little if any effect on the range of the semivariogram and the shape of it changes only slightly if checked carefully in our cases (see Supplement). The main difference between the semivariogram with and without nscoring is the y-axis, which for the nscored data is approximately scaled by the variance of the initial error data. The main difference between the method explained in this paper and the method of Rolstad et al. (2009) is the SGSim method itself.

*P4748 L19: why "or/and" ? Shouldn't it always be integrated over the largest area?*

True and this what we were trying say. Rephrased to clarify.

*P4752: L13: What percent volume change is the correction for each time period. This will just give the reader a better idea on the significance of these corrections.*

There are quite many parameters given in this table and we are therefore reluctant to add more. Among those in the current version of the table is the average lowering with and without seasonal correction which should give the reader a good indication of significance of these corrections.

*P4753 L7: Actually, the variables are not independent at all, since to calculate the volume change, you need to have the area.... But, maybe rather the results are not so sensitive to failure of the assumption....*

Well to be exact the referee is right, but the contribution to the uncertainty related to this dependence is very hard to estimate in any meaningful way. However it most likely very small.

*Table 3: place abbreviations of the parameters (table column headers) into the caption at the proper description. This will make it easier for the reader to interpret the table.*

Done.

**Reference cited here but not in the current version of the manuscript**

Berthier E., Arnaud Y., Kumar R., Ahmad S., Wagnon P., & Chevallier P., Remote sensing estimates of glacier mass balances in the Himachal Pradesh (Western Himalaya, India). *Remote Sensing of Environment*, 108(3), 327-338, doi: 10.1016/j.rse.2006.11.017, 2007

# Geodetic mass balance record with rigorous uncertainty estimates deduced from aerial photographs and LiDAR data. Case study from Drangajökull ice cap, NW-Iceland

E. Magnússon<sup>1</sup>, J. Muñoz-Cobo Belart<sup>1</sup>, F. Pálsson<sup>1</sup>, H. Ágústsson<sup>2</sup> and P. Crochet<sup>2</sup>

[1]{Institute of Earth Sciences, University of Iceland, Sturlugata 7, 101 Reykjavík.}

[2]{Icelandic Meteorological Office, Bústaðavegi 7-9, 108 Reykjavík }

Correspondence to: E. Magnússon ([eyjolffm@hi.is](mailto:eyjolffm@hi.is))

## Abstract

In this paper we describe how recent high resolution Digital Elevation Models (DEMs) can be used to extract glacier surface DEMs from old aerial photographs and to evaluate the uncertainty of the mass balance record derived from the DEMs. We present a case study for Drangajökull ice cap, NW-Iceland. This ice cap covered an area of 144 km<sup>2</sup> when it was surveyed with airborne LiDAR in 2011. Aerial photographs spanning all or most of the ice cap are available from survey flights in 1946, 1960, 1975, 1985, 1994 and 2005. All ground control points used to constrain the orientation of the aerial photographs were obtained from the high resolution LiDAR DEM. ~~(2mx2m cell size and vertical accuracy <0.5 m).~~ The LiDAR DEM was also used to estimate errors of the extracted photogrammetric DEMs in ice and snow free areas, at nunataks and outside the glacier margin. The derived errors of each DEM were used to constrain a spherical semivariogram model, which along with the derived errors in ice and snow free areas were used as inputs into 1000 Sequential Gaussian Simulations (SGSim). The simulations were used to estimate the possible bias in the entire glaciated part of the DEM as well as and. ~~The derived bias correction, varying in magnitude between DEMs from 0.03 m to 1.66 m (1946 DEM) was then applied. The simulation results were also used to calculate~~ the 95% confidence level of this bias. This, results ining bias correction varying in magnitude between 0.03 m (in 1975) and 1.66 m (in 1946) and uncertainty values between ±0.21 m (in 2005) and ±1.58 m (in 1946). Error estimation methods based on more simple proxies would typically yield 2-4 times larger error estimates. The aerial photographs used were acquired

1 between late June and early October. An additional bias correction was therefore estimated  
2 using a degree day model to obtain the volume change between the start of two hydrological  
3 years (1 October). This correction corresponds to an average elevation change of  $\sim 3.5$  m in the  
4 worst case for 1960, or ~~about~~  $\sim 32/43$  of volume change between the 1960 and the 1975 DEMs.  
5 The total uncertainty of the derived mass balance record is mostly due to uncertainty of the  
6 SGSim bias correction, the uncertainty of the seasonal bias correction and the uncertainty of  
7 the interpolated glacier surface where data is lacking. The record shows a glacier-wide mass  
8 balance rate of  $\dot{B} = -0.26580 \pm 0.040$  m w.e. a<sup>-1</sup> for the entire study period (1946-2011). We  
9 observe significant decadal variability including ~~positive~~ periods of mass gain, peaking in 1985-  
10 1994 with  $\dot{B} = 0.276 \pm 0.11$  m w.e. a<sup>-1</sup>. There is a striking difference if  $\dot{B}$  is calculated  
11 separately for the western and eastern halves of Drangajökull, with a reduction of eastern part  
12 on average  $\sim 3$  times faster than the western part. Our study emphasises the need of applying  
13 rigorous geostatistical methods for obtaining uncertainty estimates of geodetic mass balance,  
14 the importance of seasonal corrections of DEMs from glaciers with high mass turnover and the  
15 risk of extrapolating mass balance record from one glacier to another even over short distances.  
16

## 17 **1 Introduction**

18 Mountain glaciers and ice caps accounted for more than half of the land ice runoff contribution  
19 to global mean sea level rise during the 20th century (Vaughan et al., 2013). Understanding  
20 how these glaciers respond to a changing climate is essential to close the budget of the sea-level  
21 rise over the last decades and project the sea-level rise in the near future. In recent years an  
22 increased part of our knowledge on how these glaciers are changing has been based on remote  
23 sensing. The majority of these studies describe current or recent glacier changes in different  
24 parts of the globe applying geodetic methods (Gardelle et al., 2012; Berthier et al., 2010). Others  
25 have presented results on the geodetic mass balance extending further back (e.g. Fischer et al.,  
26 2015; Nuth et al., 2007; Soruco et al., 2009); ~~but~~ these studies are particularly important since  
27 they indicate how the glaciers responded to 20th century climate variability. Such observations  
28 can be used to constrain or correct glacier mass balance models that are used to estimate how  
29 the glaciers will respond to future climate changes (e.g. Clarke et al., 2015).

30 Studies on long term geodetic mass balance are generally based on digitised contour maps, with  
31 some exceptions where mass balance records have been derived from Digital Elevation Models  
32 (DEMs) extracted from old archives of aerial photographs applying digital photogrammetry

1 (e.g. James et al., [2006](#); 2012). The applicability of geodetic mass balance records as a key to  
2 predicting future glacier changes depends on the accuracy of such records and their resolution.  
3 To maximize both the accuracy and the resolution we should rather focus, if possible, on  
4 archives of aerial photographs, because:

5 i) These archives often span more epochs than the published topographic maps.

6 ii) With new and rapidly improving tools in digital photogrammetry the potential to produce  
7 much more accurate and detailed DEMs than those deduced by interpolating elevation contours  
8 from old maps has increased significantly.

9 iii) The availability of high resolution DEMs has opened a new source of ground control points  
10 (GCPs) for constraining the orientation of photogrammetric DEMs ([James et al., 2006](#); Barrand  
11 et al., 2009). Like ii), this will lead to more accurate DEMs from aerial photograph archives in  
12 future studies. New spaceborne sensors such as Worldview and Pléiades may allow such studies  
13 in remote areas without conducting expensive field campaigns to survey GCPs ([Papasodoro et](#)  
14 [al., 2015](#)).

15 In order to maximize the value of geodetic mass balance records, realistic uncertainty  
16 assessments are required. If the uncertainty is overestimated, the value of the information that  
17 we can extract from the geodetic data will be diminished, the results will be neglected by the  
18 scientific community or not even be published. If, however, the uncertainty is underestimated,  
19 geodetic mass balance records with significant errors will be interpreted as solid observations.  
20 When extracting volume change from two different DEMs a common approach is to use the  
21 standard deviation of the DEM difference in the unglaciated part of the DEMs as a proxy for  
22 the uncertainty of the average elevation change (e.g. Cox [and Marchet-aland](#), 2004). This  
23 method corresponds to an extreme case, assuming that the errors of the surface elevation change  
24 are totally correlated between all grid cells within the glacier. The opposed extreme case  
25 assuming that the errors of surface elevation change are totally uncorrelated between all grid  
26 cells has also been applied in the literature (e.g. Thibert et al., 2008). This approach results in  
27 an estimated uncertainty reduced by a factor  $\sqrt{n}$  compared to the totally correlated uncertainty  
28 where n is the number cells for which the difference is calculated. The third alternative, where  
29 the spatial dependence of the DEM errors is estimated and inherent in the uncertainty estimate,  
30 was described by Rolstad et al. in 2009. This method results in uncertainty somewhere between  
31 the two extremes and has been adopted in several studies (e.g. Trüssel et al., 2013; Zemp et al.,

1 2013; Fischer et al., 2015). This method includes some simplifications, which so far have not  
2 been validated with other geostatistical methods.

3 Here, we present a case study of Drangajökull ice cap in NW-Iceland (Fig. 1) based on seven  
4 sets of aerial photographs in 1946-2005 and a LiDAR DEM obtained from an airplane in 2011  
5 (Jóhannesson et al., 2013). The glacier covered an area of 144 km<sup>2</sup> in 2011 and is the 5th largest  
6 glacier in Iceland. This study describes an alternative method to estimate uncertainties of the  
7 average elevation change derived by differencing DEMs, applying geostatistical methods. The  
8 approach, which uses the DEM difference from ice and snow free areas as input, allows for a  
9 simultaneous estimate of a bias correction for the glaciated part of the DEMs. Both the  
10 estimated uncertainty and the bias correction are compared with results from conventional  
11 methods. We also interpolate volume changes in areas where data is lacking and inspect how  
12 much of the derived volume change may be caused by seasonal variation. The study results in  
13 a seasonally corrected mass balance record of Drangajökull ice cap with estimates of possible  
14 errors contributing to the record as well as the derived net uncertainty. ~~Finally, we present a  
15 simple mass balance model, scaled with the geodetic mass balance results, revealing annual  
16 values of glacier-wide winter, summer and net mass balance of Drangajökull in 1958-2011.~~

17

## 18 **2 Data and methods**

19 In this study, seven sets of aerial photographs covering Drangajökull ice cap in 1946, 1960,  
20 1975, 1985, 1986 and 1994 from the archives of the National Land Survey of Iceland,  
21 Landmælingar Íslands, and in 2005 from Loftmyndir ehf were used. Negative films were  
22 scanned with a photogrammetric scanner in a resolution of 15 µm and 20µm. The aerial  
23 photographs have an average scale between ~1:30000 and ~1:40000, which result in a Ground  
24 Sampling Distance (GSD) of ~0.4 m to ~1 m. Complete camera calibration information is  
25 available for the surveys of 1975, 1985, 1986, 1994 and 2005, but calibration information is  
26 lacking for the oldest flights (1946 and 1960). Only the focal length is available for the  
27 photographs of 1946, and focal length and radial distortion are available for the photographs of  
28 1960. Table 1 summarizes the main characteristics of each series.

29 During the International Polar Year (IPY) 2007–09, a major effort was initiated to produce  
30 accurate DEMs of all the major Icelandic glaciers and ice caps (Jóhannesson et al., 2013). In  
31 July 2011 Drangajökull ice cap was surveyed with high airborne LiDAR model Optech ALTM  
32 3100. resolution airborne LiDAR. The LiDAR DEM covers the entire ice cap as well as the  
33 close vicinity of the glacier, which provides a useful reference to constrain and validate the

1 other DEMs produced in this study. Specifications of the survey are described in Jóhannesson  
2 et al., 2013. The average density of the point cloud measured with the LiDAR corresponded  
3 0.33 hits m<sup>-2</sup>. The high density facilitates a well constrained bi-linear interpolation of the point  
4 cloud into a grid with 2mx2m cell size. Nodes/Cells where the distance to nearest LiDAR  
5 hit exceeds 4 m were masked out. The point cloud from the survey was used to produce a high  
6 resolution DEM (2mx2m cell size). A comparison of differential GPS profiles and 5mx5m grid  
7 derived from identical Lidar survey in the Snæfelljökull ice cap in western Iceland indicated  
8 vertical accuracy well within 0.5 m with an estimated vertical accuracy well within 0.5 m  
9 (Jóhannesson et al., 2011). The LiDAR data for Drangajökull was acquired through an effort,  
10 initiated during the International Polar Year (IPY) 2007–09, to produce accurate DEMs of all  
11 the major Icelandic glaciers and ice caps (Jóhannesson et al., 2013). The derived DEM covers  
12 the entire ice cap as well as the close vicinity of the glacier, which provides a useful reference  
13 to constrain and validate other DEMs produced in this study.

## 14 **2.1 Creation of DEMs and orthorectified photographs**

15 The DEMs were created from the aerial photographs using the software bundle IMAGINE  
16 Photogrammetry (© Intergraph). The photogrammetric processing is carried out in four steps:  
17 Orientation of the images, automatic stereo matching, manual editing of the DEMs and  
18 orthorectification of aerial photographs.

19 Each series of aerial photographs was oriented individually by means of a rigorous bundle  
20 adjustment (Wolf and Dewitt, 2010). The glacier is covered by a single series of images for all  
21 years except in 1960 when the glacier was covered by three tiles, one per date (Table 1). Tie  
22 points were automatically measured in the images and semi-automatically revised, ensuring a  
23 good connection between all the adjacent photographs and between strips. The exterior  
24 orientation was constrained by using series of Ground Control Points (GCPs) extracted from  
25 the LiDAR DEM (2mx2m cell size) applying a similar in a similar approach as to the one carried  
26 out by James et al. (2006). The LiDAR DEM was viewed as a hillshade with approximately the  
27 same similar sun position/light conditions as during the acquisition of the photographs. This  
28 allowed recognition of and extraction of GCPs from stable features such as boulders and sharp  
29 edges in the ice-free areas in the vicinity of the ice cap and at nunataks (Fig. 2). To ensure  
30 stability in the orientation a fairly regularly distribution of GCPs over the photographed area as  
31 well as over the elevation span of the terrain is required. The location- (Kraus, 2007; Nuth and  
32 Kääb, 2011). Artificial dip or rise in the DEM due to insufficient coverage of GCPs would skew  
33 the geodetic mass balance record and make its uncertainty estimate explained below less valid

1 (further explained in Sect. 2.2). -In our case the nunataks of Drangajökull ice cap secure allows  
2 fairly even spatial and vertical distribution of GCPs for all epochs (GCP locations shown for  
3 each DEM in Fig. 2). The photogrammetric orientations performed in this study never span  
4 more than 2 photographs without having constraints from a GCP. This is considered as  
5 sufficient coverage of GCPs for a reliable orientation (Kraus, 2007). The assigned uncertainty  
6 of the GCPs used in the DEM processing was 2 m standard deviation in XY and 0.5 m for Z  
7 corresponding respectively to the Lidar DEM resolution and expected vertical accuracy. A  
8 significant part the large scale errors in the derived photogrammetric DEM may be related to  
9 errors in the GCPs 3D locations, particularly for DEMs from 1975 and later when other data  
10 constraining the geometric model are relatively accurate.- For the 1946 and 1960 DEMs a lack  
11 of camera calibration information is likely to be a more important source of errors. of GCPs  
12 was based on a regular scheme of distribution surrounding and inside the area of interest in  
13 order to ensure stability in the orientation over the entire study area (Kraus, 2007).

14 The orientation of the 1960 images was carried out using the focal length and lens distortion  
15 information obtained from the calibration report of the DMA Cameras (Spriggs, 1966). The  
16 1946 images included information of the focal length written at the margin of the first image of  
17 each strip. Both cases needed auxiliary pre-calibration, therefore pseudo-fiducial marks were  
18 created allowing the location of a pseudo-principal point (see e.g. Kunz et al., 2012, for details).  
19 The orientation of both sets of images included additional parameters in the bundle adjustment  
20 for refinement of the camera geometry. Bauer's model (Bauer and Müller, 1972) was used for  
21 the images of 1946 and Jacobsen's model (Jacobsen, 1982) was used for the images of 1960.

22 Once oriented, we produced the elevation point clouds from stereo-matching of the images. The  
23 routine eATE (enhanced Automatic Terrain Extraction) of the software allows for a pixel-wise  
24 evaluation in the matching process, thus obtaining a high density of points. The low-contrast in  
25 firn and snow covered areas caused failures in the matching process. The point clouds for low-  
26 contrast areas were therefore created from reduced resolution of the stereo images and a larger  
27 windows size and lower correlation coefficient of the stereo matching. This resulted in an  
28 improved coverage of points automatically measured in the snow-covered areas. with a  
29 configuration based on matching in lower resolution of the images and using larger windows  
30 size and lower correlation coefficient. A first edition of the point clouds was carried out with  
31 the software CloudCompare (GPL Software); automatic outlier filtering removal was  
32 performed from the PCL plugin using the routine "Statistical Outlier Removal" (Rusu et al.,  
33 2011). and tThe dense point clouds were then subsampled in regular density of points

1 corresponding to ~10mx10m spacing (series of 1960, 1975, 1994 and 2005)for all epochs  
2 except 1946 and 1985 for which density ~~is~~equivalent to ~20mx20m spacing was applied. This  
3 was done to -reduceing the size of the point clouds and removeing double points that could  
4 introduce noise when interpolating the point clouds as a grid with fixed cell size (Sect. 2.2 and  
5 2.3). The lower subsampled point density was due to large GSD in the case of 1946 and high  
6 level of noise in the images in 1985, resulting in large amount of outliers. Finally a thorough  
7 maual revision of the results in stereoscopic vision was carried out, ~~manually~~ editing the DEMs  
8 in the glacier areas where the automatic matching failed and surface details were still  
9 perceptible.

10 To delineate the glacier margin and mask out snow covered areas (Sect. 2.2 and 2.4)  
11 orthorectified photographs were required. The orthorectification was carried out using  
12 preliminary DEMs linearly interpolated from the point clouds as grids with 10mx10m (DEMs  
13 of 1960, 1975, 1994 and 2005) and 20x20m cell size (DEMs of 1946 and 1985). The series of  
14 1975 included 2 strips finishing on the glacier (Fig. 2) without covering completely the glacier  
15 in stereo. These images were orthorectified using the LiDAR DEM, revealing the location of  
16 the glacier margin at its intersection with the bare ground, free of ice and ~~s~~now in both 1975  
17 and 2011 (resulting in insignificant elevation change at the 1975 margin location in this  
18 area).~~When monoscopic coverage was only available, the LiDAR DEM was used for the~~  
19 ~~orthorectification, revealing accurately the location of the glacier margin.~~ The orthorectification  
20 of all the series of photographs was performed in resolution corresponding to a 2mx2m pixel  
21 size.

## 22 **2.2 DEM error assessment and bias correction**

23 We use the high resolution LiDAR DEM obtained in 2011 to assess the quality of the  
24 photogrammetric DEMs. The photogrammetric DEMs are expected to be of significantly worse  
25 quality in terms of accuracy than the LiDAR data and we therefore assume for simplicity that  
26 statistical parameters derived from the difference between the photogrammetric DEM and the  
27 LiDAR DEM (in areas assumed stable) describe errors in the photographic DEM. This is likely  
28 to produce a minor underestimate of the actual quality of the photographic DEMs. As described  
29 below, all photogrammetric DEMs were bias corrected relative to the LiDAR DEM. A possible  
30 bias in the absolute location of the LiDAR DEM does not affect our result since this the bias is  
31 cancelled out when calculating the difference between the DEMs.

32 The first step in estimating the quality of a DEM derived from the aerial photographs was  
33 calculating the difference between the photogrammetrically ~~deduced~~derived point clouds (Fig.

1 S1 in ~~S~~supplementary data) and ~~the~~ LiDAR DEM with 2mx2m cell size. This was calculated  
2 using the residual operation in Surfer 12 (©Golden Software, Inc). From this a digital model of  
3 the difference between the DEMs was ~~calculated and~~ linearly interpolated ~~for a grid with~~  
4 ~~20mx20m cell size. All cells~~ with snow or glacier cover at either or both dates (photograph and  
5 LiDAR acquisitions) were masked out as well as cells~~in the difference model\_ where\_ distance~~  
6 ~~to the next element of the point cloud exceeds 40 m. were masked out as well as cells where we~~  
7 ~~expect actual surface changes between the dates of photograph and LiDAR acquisitions. This~~  
8 ~~includes areas which are glaciated and snow covered at either or both dates.~~ The glacier outlines  
9 were delineated manually (see Sect. 2.4) and the snow covered areas were derived with  
10 semiautomatic classification of the orthorectified aerial photographs and the intensity images  
11 derived from the LiDAR scanning. The mean and the standard deviation ( $\sigma$ ) of the derived  
12 difference (photogrammetric DEM - LiDAR DEM) of the remaining data after snow and glacier  
13 masking is ~~tabulated shown~~ in Table 2.

14 Extraction of geodetic mass balance requires co-registered DEMs prior to calculation of glacier  
15 volume changes. This usually includes estimates of relative vertical and horizontal shift  
16 between the DEMs using areas where the elevation change is expected to be insignificant  
17 (Kääb, 2005; Nuth and Kääb, 2011; Guðmundsson et al., 2011). In this study the GCPs used  
18 during the orientation of the photographs were extracted from the LiDAR DEM in maximum  
19 resolution (2mx2m cell size). We were able to extract several GCPs at nunataks near the glacier  
20 centre. The distribution of GCPs is therefore fairly regular over the survey area in all cases both  
21 spatially (Fig. 2) and with elevation. The orientation of aerial photographs resulted in horizontal  
22 RMSE of the GCPs <3m in all cases, and typically 1-2 m (Table 2). These values are obtained  
23 from least square adjustment resulting in residual mean equal to zero. The horizontal shift  
24 relative to the LiDAR DEM is likely to exceed the derived horizontal RMSE locally for a given  
25 photogrammetric DEM. It is however ~~very~~ unlikely that the average horizontal shift relative to  
26 the LiDAR DEM exceeds the derived horizontal RMSE~~shift~~ of the GCPs. ~~We therefore~~  
27 concluded that horizontal shift corrections are not required for the photographic DEMs.

28 ~~To compensate for slowly varying errors in the DEM difference the~~ The elevation difference  
29 between DEMs ~~in~~covering stable areas is commonly used to estimate zero order (bias  
30 correction, see e.g. Nuth and Kääb, 2011; Guðmundsson et al., 2011) or higher order correction  
31 (e.g. Rolstad, 2009; Nuth and Kääb, 2011) to compensate for slowly varying errors in DEM  
32 difference over glaciated areas. The result from such approach is, however, sensitive to the area  
33 chosen as the reference area. One can choose to use the entire area covered by both DEMs

1 outside the glacier or an area limited by a certain distance from the glacier. In this study we  
2 apply geo-statistical methods for deriving bias correction of each photogrammetric DEM within  
3 the glacier and an estimate of the uncertainty in the derived bias correction. These calculations  
4 consisted of five main steps:

5 1) Preparation of DEM error input data (derived from the comparison with the LIDAR),  
6 explained below. Resulting error data from ice and snow-free areas is shown in Fig. 3.

7 ~~2) Calculation of transform function, Transformation of the derived DEM errors into a new~~  
8 ~~variable with the nscore function (Deutsch and Journel, 1998) in WinGSLib V.1.5.8 (© Statios~~  
9 ~~LLC). The histogram of the new variable fits modifying the input data in such way that its~~  
10 ~~histogram a fits~~ normal distribution, with zeros mean and  $\sigma=1$ . ~~This step is a recommended~~  
11 ~~preparation of a dataset for valid Sequential Gaussian Simulation (SGSim) carried out in step 5~~  
12 ~~particularly if the histogram of the DEM error does not close toly resemble a normal~~  
13 ~~distribution., and transformation of the input data accordingly using the nscore function~~  
14 ~~(Deutsch and Journel, 1998) in WinGSLib V.1.5.8 (© Statios LLC).~~

15 3) Calculation of semivariogram for the nscored input data, ~~in which the~~ but semivariogram  
16 describes the variance,  $\gamma$ , of a given coordinate-based variable as a function of distance,  $d$ ,  
17 between sampled locations.

18 4) Calculation of a spherical semivariogram model, fitting the derived semivariogram.

19 5) Use of the derived spherical model and the nscored data that constrain the semivariogram to  
20 run 1000 Sequential Gaussian Simulation (SGSim) of the nscored errors in the glaciated areas  
21 using the sgsim function (Deutsch and Journel, 1998) in WinGSLib. The sgsim function includes  
22 reversed transformation from the nscored variable to the derived DEM error. SGSim are  
23 commonly applied in errors assessments of geo-statistical studies (e.g. Lee et al., 2007;  
24 Cardellini et al., 2003). The results from the sgsim runs were used to estimate both the most  
25 likely bias of each photogrammetric DEM within the glacier and 95% confidence level of this  
26 bias, as explained further below.

27 The approach adopted here requires that the statistics of the DEM errors outside the glacier are  
28 descriptive for the errors in the photogrammetric DEM within the glacier margin. This should  
29 be kept in mind, both during the photogrammetric processing and in the preparation of input  
30 data (step 1) used in the geo-statistical calculation. The photogrammetric processing requires  
31 fairly even spatial distribution of GCPs, otherwise artificial dip or rise in the photogrammetric  
32 DEM are likely to be produced in areas far from a GCP (Kraus, 2007). Such errors would not

1 be represented in a semivariogram based on DEM error in areas where distribution of GCPs is  
2 ~~much betteradequate. In our case the nunataks of Drangajökull ice cap secure fairly even~~  
3 ~~distribution of GCPs (Fig. 2). The photogrammetric orientations performed in this study never~~  
4 ~~span more than 2 photographs without having constraints from a GCP. This is considered as~~  
5 ~~sufficient coverage of GCPs for a reliable orientation (Kraus, 2007).~~

6 The low contrast of snow covered glacier surface may also result in a difference in error  
7 statistics between the glacier and the ice and snow free areas (Rolstad et al., 2009). The low  
8 contrast should mostly produce high frequency errors, whereas low frequency errors are mostly  
9 caused by an inaccurate orientation. The eATE configuration used resulted in fewer but better  
10 matching points in the low-contrast areas (Sect. 2.1) and the thorough manual 3D revision likely  
11 removes most of the high frequency noise in the resulting DEM. A semivariogram of the  
12 difference between the point cloud in 1946 at low contrast glacier areas and the LiDAR DEM  
13 (blue crosses in Fig. 4c) reveals the variance with distance for the elevation error plus the  
14 elevation changes in 1946 to 2011. The variance of elevation changes over short distance should  
15 be small for smooth glacier surface. At short distances the semivariogram should therefore  
16 mainly represent the DEM errors. shows variance fFor  $d < 200$  m the low contrast areas show  
17 variance at similar level as for the DEM error data outside the glacier (Fig. 4c) indicating similar  
18 level of high frequency error for the two area types. Both cases reveal the dependency of the  
19 errors in the 1946 DEM over short distances since variation in elevation changes on the glacier  
20 over distances  $< 200$  m are generally small. This supports that the errors in low contrast area are  
21 unlikely to skew significantly our geo-statistical analyses.

22 A difference in terrain slope between areas can produce a significant difference in the calculated  
23 semivariogram (Rolstad et al., 2009). Local horizontal shift between DEMs can produce  
24 significant artificial elevation difference in steep areas. The average slope on the glacier in 2011  
25 was  $6.2^\circ$  whereas the unglaciated area in the 2011 LiDAR DEM had an average slope of  $9.8^\circ$ .  
26 The preparation of our data (step 1) therefore includes exclusion of all data where slope exceeds  
27  $20^\circ$ ; ~~but~~ unglaciated areas in the 2011 LiDAR DEM, ~~fulfilling this criteria~~ below this slope  
28 limit has an average slope of  $7.2^\circ$ .

29 The glaciated parts of the photogrammetric DEMs were all manually revised using 3D vision,  
30 securing removal of significant outliers within the glacier. A thorough revision was not carried  
31 out for the unglaciated areas. Instead we apply automatic removal of outliers. This was carried  
32 out by calculating standard deviation of the DEM error (photogrammetric DEM- LiDAR  
33 DEM),  $\sigma_{\epsilon h}$  (after masking out snow-covered, glacier-covered and steep areas) and filtering the

1 DEM difference with a 500mx500m median filter. Values where the difference between the  
 2 unfiltered and the median filtered value DEM difference exceeded  $\sigma_{\varepsilon_h}$  were then masked out.  
 3 The mean DEM error and  $\sigma_{\varepsilon_h}$  after the slope and outlier masking is shown in Table 2.

4 The semivariograms obtained with (step 3) and without the nscore transformation of the 1946  
 5 DEM error in ice and snow free areas are shown in Fig. 4a-b. The spherical semivariogram  
 6 model calculated in step 4 is given as function of  $d$  (distance between sampled locations):

$$\begin{aligned}
 7 \quad \gamma(d) &= 0 & d &= 0 \\
 8 \quad &= c_0 + c_1 \left[ \frac{3d}{2r} - \frac{1}{2} \left( \frac{d}{r} \right)^3 \right] & 0 < d \leq r \\
 9 \quad &= c & d > r & \quad (1)
 \end{aligned}$$

10 ~~where~~  $c = c_0 + c_1$  and  $\gamma(0)$  describes the correlation of a point with itself. The main parameters  
 11 in the model, nugget ( $c_0$ ), range ( $r$ ) and sill ( $c$ ) are shown in the Fig. 4b. We expect  $c$  to equal  
 12 approximately the global variance of the data set, hence  $c \sim 1$  for the nscored data. The shape  
 13 of the semivariograms that we obtain (Fig. 4a-b and Fig. S2 in supplementary data) indicate a  
 14 reasonable fitting with a single spherical model unlike in the study by Rolstad et al., (2009)  
 15 where two spherical models describing the variance at different ranges of distances were  
 16 required.

17 The size of the DEM error grid (in full resolution (20mx20m cell size) was too large for the  
 18 sgsim function to operate (step 5). The data size was reduced by picking out every 5<sup>th</sup> column  
 19 and line in the DEM error grid. In areas where data was sparse, at nunataks and where few data  
 20 points remained due to the snow mask near the glacier margin, the 20mx20m data was used.  
 21 Tests with smaller study areas indicated that this reduction of the input data only have minor  
 22 effects on the results derived from the simulation.

23 Each SGSsim, constrained by the input data and the spherical semivariogram model and  
 24 calculated in resolution corresponding to 100mx100m cell size, reveals possible errors in the  
 25 measured glaciated area of the examined photogrammetric DEM. From each simulation the  
 26 mean error of the glaciated area was calculated. From the 1000 simulations a histogram was  
 27 derived and used to approximate a probability function of the likely bias in glaciated part of the  
 28 DEM. Figure 4f shows the derived histogram for the 1946 DEM. It also shows the mean (Fig.  
 29 4d) and  $\gamma$  (Fig. 4e) of the derived error from 1000 simulation at each cell of the simulated area  
 30 within the glacier. The latter reveals how the uncertainty in the derived error increases with  
 31 distance from the input data. This should reach a maximum at a distance corresponding

1 approximately to the range ( $r$ ) in the spherical semivariogram model, but all points on glacier  
2 in the 1946 DEM are at distance  $<r$  from input data. The spatially varying mean error (Fig. 4d)  
3 could be used directly for correction of the photographic DEM, but instead we subtract the  
4 mean of the derived probability function to bias correct the area of interest in the  
5 photogrammetric DEM. Both approaches would lead to same result when deducing volume  
6 changes from the DEM differencing. The derived bias,  $z\_bias$ , used to correct each DEM, and  
7 the corresponding 95% upper ( $z\_bias_u$ ) and lower confidence limits ( $z\_bias_l$ ), is tabulated in  
8 Table 2. For comparison purposes the table also shows error bars derived by calculating  
9 analytically the expected variance ( $\sigma_{z\_bias}^2$ ) in the DEM error averaged over circular region  
10 corresponding to the size of Drangajökull, using a spherical semivariogram model (Rolstad et  
11 al., 2009), which fits the semivariogram without nscoring the error input data (Fig. 4a).

### 12 **2.3 Finalizing the glacier DEMs**

13 The photogrammetrically derived point clouds are typically much less dense for the snow  
14 covered glacier surface than for bare ice or outside the glacier ground (see Supplement). The  
15 typical distance between points on the snow covered glacier surface -in the 1946 point cloud  
16 (the worst dataset in terms of noise and point density) is  $\sim 100$  m, corresponding approximately  
17 to the resolution of the SGSim carried out. The point density is poorer for limited areas and in  
18 some regions ~~there are~~ gaps in the point clouds are caused by lack of contrast. Interpolating the  
19 elevation point clouds directly over long distances can be risky due to the spatial variability of  
20 the elevation. The spatial variability of the elevation changes derived from the difference  
21 between the point cloud and the LiDAR DEM is expected to be much lower (Cox and March,  
22 2004). Therefore the bias corrected difference was interpolated (Sect. 2.2) and added to the  
23 LiDAR DEM. The kriging function in Surfer 12 (©Golden Software, Inc.) was used to  
24 interpolate the data applying default linear variogram model and data search radius of 500 m.  
25 Even though the elevation changes compared to LiDAR are expected to be spatially smooth,  
26 interpolation over longer distance would reduce the reliability of the uncertainty assessment  
27 carried out for the photogrammetric~~phie~~ DEMs. The different interpolation methods used  
28 within (kriging) and outside (linear) the glacier produces minor difference in the error statistics.  
29 For the 1946 bedrock data (after slope and outlier masking)  $\sigma$  is 4.80 m and 4.79 m for the  
30 linear and kriging methods respectively but 4.77\_m derived directly from the point cloud  
31 difference compared to the full resolution LiDAR DEM.

32 The resulting grids of elevation changes relative to LiDAR contained some larger gaps due to  
33 lack of contrast, cloud cover or incomplete coverage of aerial photographs for all datasets

1 except the one of 2005 (Table 2). To complete the difference maps two main interpolation  
2 methods were used: For relatively small gaps, spanning short elevation range, kriging  
3 interpolation with data search radius  $>500$  m was applied using the derived elevation difference  
4 at the boundary of the data gap as input. For larger areas spanning significant elevation range  
5 we estimated a piecewise linear function for the elevation change as function of the 2011  
6 elevation (at 100 m elevation intervals) using the elevation difference between the point cloud  
7 and the LiDAR DEM as input (see supplementary data). For data gaps covering an area at both  
8 the east and west side off the glacier the two different interpolations were carried out, one for  
9 the area west of the ice divides and another for the area east of it. In four cases neither of the  
10 above interpolation methods were considered applicable. The approaches adopted for each of  
11 these cases is described in the supplementary data. The location of data gaps are shown in Fig.  
12 S1 and the interpolation method applied in each case is shown supplementary data.

13 The uncertainties associated with interpolation of data gaps in the DEMs was approximated  
14 independently from the uncertainties of measured photogrammetric DEMs (Sect. 2.2). It is  
15 difficult to quantify these errors, but since these areas are generally small relative to the  
16 measured areas we adopted a generous approximation of the uncertainty roughly based on the  
17 scatter of the elevation change with altitude (point clouds compared to LiDAR DEMs). We  
18 assign three values of elevation uncertainty (95% confidence level) to the interpolated areas,  
19  $\pm 7.5$  m,  $\pm 10$  m and  $\pm 15$  m, depending on the quality of the input data used for the interpolation  
20 and the applicability of the interpolation method (for further details see supplementary data).  
21 The interpolated areas with the highest uncertainties were adopted for the lowermost part of  
22 Leirufjarðarjökull that was not covered in the 1975 survey flight (see supplementary data). Also  
23 a relatively large area in southernmost part of Drangajökull in 1946 where the interpolated area  
24 is poorly constrained by data. Cluster of nearby data gaps are considered as single area with  
25 assigned elevation uncertainty. We however assume that the error in one area is independent  
26 from the elevation error in other areas due to the distance between them.

## 27 **2.4 Delineating glacier margins and nunataks**

28 The glacier margin and nunataks at each time were delineated manually using the orthorectified  
29 aerial photographs at given time as well as the derived elevation difference compared to the  
30 LiDAR DEM. For 2011 the glacier outlines were drawn based on a shaded relief image of the  
31 2011 DEM in maximum resolution and the intensity image of the LiDAR measurements. All  
32 glacier margins were delineated by the same person. The glacier margin was therefore  
33 interpreted in similar manner for all years, in areas where the outlines are uncertain. This

1 working procedure minimizes variations in relative area changes of the ice cap. Due to  
2 numerous firn patches in the vicinity of Drangajökull, some of which are connected to the ice  
3 cap, it is actually a matter of definition if these connected patches should be included as part of  
4 Drangajökull or not. We follow the approach of Jóhannesson et al. (2013) and exclude these  
5 patches. In a few areas the aerial photographs do not always reveal the glacier margin. This  
6 includes the southernmost part of Drangajökull in 1946. In this area the location of the glacier  
7 margin has been very stable since 1960. We therefore adopted at each location, the outermost  
8 glacier margin in the 1960-2011 datasets, as the 1946 margin in this area. Data used to  
9 approximate the location of the glacier margin in other areas where data is absent is described  
10 in the supplementary data. The evolution of the glacier area is shown in Fig. 5. Also shown in  
11 Fig. 5 is the area of the eastern and western sections of the glacier, when Drangajökull is divided  
12 in two along the ice divides from north to south (see Fig. 6).

## 13 2.5 Calculating volume changes

14 To derive the volume change,  $\delta V(t_s, t_f)$ , of the ice cap during a period  $t_s-t_f$ , the elevation  
15 difference  $DEM_f-DEM_s$  (Fig. 6), was integrated over the area covered by glacier at either or  
16 both DEM dates  $t_s$  or/and  $t_f$ . A continuous DEMs and glacier outlines had been completed for  
17 all years except for the year 1994, but this data set covered only  $\sim 2/3$  of Drangajökull glacier  
18 with the southernmost third of the ice cap missing. In order to estimate volume changes for this  
19 part of the glacier in the periods 1985-1994 and 1994-2005 the volume changes for the  
20 southernmost third of the glacier were plotted as function of deduced volume changes in the  
21 other  $\sim 2/3$  of the glacier for the periods 1960-1975, 1975-1985, 1985-2005 and 2005-2011 (Fig.  
22 7). Linear fit describing relation between the volume changes in the two areas estimated with  
23 least-squares was used to estimate volume changes for the southern part of the glacier in the  
24 period 1985-1994 and 1994-2005. Errors in these volume change estimates were approximated  
25 using the 95% confidence level of the linear fit (estimated in Grapher 10 ©Golden Software,  
26 Inc.). Instead of approximating the position of the 1994 glacier margin, we only approximated  
27 the area covered by this part of the glacier. The volume change for the southernmost part of  
28 Drangajökull in the periods 1975-1985 was approximately the same as the estimated volume  
29 change in 1985-1994. We therefore extrapolate the  $0.7 \text{ km}^2$  area increase of this glacier part of  
30 in 1975-1985 to the period 1985-1994 to estimate the area of this glacier part in 1994.

## 2.6 Seasonal correction of volume change between DEMs

The DEMs of Drangajökull were extracted from data acquired at different dates during the summer or the autumn (Table 1). Deriving mass balance records from DEM difference without taking this into the account will skew the results, particularly if the acquisition time of the DEMs differs much from one DEM to another; ~~ideally DEMs at the start of each glaciological year should be used.~~ Seasonal correction (sometimes referred to as date correction) have been applied and discussed in numerous studies (e.g. Krimmel, 1999; Cox and March, 2004; Cogley, 2009). -In this study the derived volume change in between DEMs ( $\delta V(t_s, t_f)$ , in Sect. 2.5) was seasonally corrected by compensating for the expected volume change of the ice cap from the acquisition date of each DEM until the end of the glaciological year (1 October). The end of the glaciological year was chosen because it makes comparison with both mass balance records and meteorological data easier and more eligible. This choice results in larger magnitude of seasonal correction (and consequently larger uncertainty estimates), when compared to the average acquisition date of the DEMs. The seasonally corrected volume changes is given by

$$\delta V^*(t_s, t_f) = \delta V(t_s, t_f) + \delta V_{S\_cor}(t_s) - \delta V_{S\_cor}(t_f) \quad (2)$$

The expected volume changes,  $\delta V_{S\_cor}$  from the time of data acquisitions  $t_a$  until the end of the glaciological year  $t_{end}$  was estimated using positive degree day ( $T_+$ ) model (e. g. Jóhannesson et al., 1995) with a constant degree day factor ( $ddf$ ) for the whole ice cap:

$$\delta V_{S\_cor} = \frac{1}{c_{\delta V_{S\_cor}}} \cdot ddf \sum_{t_a}^{t_{end} \text{ glacier}} \int T_+(t, x, y) dA \quad (3)$$

Where  $c_{\delta V_{S\_cor}}$  is the conversion factor from the glacier volume change during the period  $t_a$ - $t_{end}$  to the melt water draining from the ice cap in the same period. For seasonal volume correction of the DEM in 1960 to 2011, 1975, 1985, 1994, and 2005 DEMs we use daily grids of temperature at 2 m height above ground available ~~for the period 1949-2010~~ back to 1949 (Crochet and Jóhannesson, 2011; unpublished data of the Icelandic Meteorological Office, for the year 2011). The grids were derived in two steps: i) Applying tension spline interpolation of measured temperature at meteorological stations corrected with fixed lapse rate to represent

1 temperature at sea level. ii) Lapse rate adjustment ( $6.5^{\circ}\text{C km}^{-1}$ ) of interpolated temperature to  
 2 compensate for the effects of topography. The temperature grids were in 1 km x 1 km cell size,  
 3 but we linearly interpolated the grid in same resolution as the DEMs we are working with  
 4 (20mx20m cell size). ~~The model was scaled to fit the water equivalent of the net glacier volume~~  
 5 ~~change ( $\delta V$ ) in 1960 to 2005 without any seasonal correction. Assuming that the~~  
 6 ~~accumulation/ablation integrated over glacier surface during this time period equals the total~~  
 7 ~~winter precipitation/summer melting ( $P_w/M_s$ ) within the glacier margin we get~~

$$8 \quad c_{\delta V} \cdot \delta V(1960,2005) = P_w(1960,2005) - M_s(1960,2005) \quad (4)$$

11 where

$$13 \quad P_w(1960,2005) = \sum_{t_{1960}}^{t_{2005}} (1-S) \int_{-}^{glacier(t)} p(t,x,y) dA \quad (5)$$

15 and

$$17 \quad M_s(1960,2005) = ddf \sum_{t_{1960}}^{t_{2005}} S \int_{-}^{glacier(t)} T_+(t,x,y) dA \quad (6)$$

19 The conversion factor  $c_{\delta V}$  is assumed to be 0.85 (Huss, 2013).  $p$  is daily values of precipitation.  
 20  $S=1$  from 21 May to 30 September each year, but 0 otherwise, defining the melt season. The  
 21 definition of summer start is the day of year when the average temperature on the glacier  
 22 (derived from the interpolated daily temperatures) has on average (in 1949-2010) reached a  
 23 positive value. At the start of the glaciological year (1 October) this temperature is  $\sim 0^{\circ}\text{C}$ .  
 24 Around 1/3 of 1960 DEM was acquired  $\sim 3$  weeks earlier than the rest (Table 1). The positive  
 25 degrees in between the two acquisitions were simple given the weight 1/3 (same applies to the  
 26 1960 seasonal correction). For area integration of  $p$  and  $T_+$  the glacier area changes stepwise at  
 27 the mid of each period defined by the DEMs dates.

1 The daily precipitation data was derived from two sources. The former, referred to as  $p_1$ , was  
2 daily precipitation maps (1 km x 1 km cell size) in 1958-2006 deduced from ERA-40 (Uppala,  
3 2005) by dynamic downscaling with linear model of orographic precipitation (an update of  
4 Crochet et al. (2007) described in Jóhannesson et al. (2007)). The latter, referred to as  $p_2$ , is  
5 daily precipitation maps (1 km x 1 km cell size) for the period 1991-2012 constructed by  
6 combining wind-loss corrected rain-gauge measurements and long-term averaged monthly  
7 precipitation maps derived from the LT-model ( $p_1$ ) through a two-step anomaly mapping  
8 method (Crochet, 2013). Comparisons made at the Icelandic Meteorological office of the  
9 former record with runoff from Hvalá drainage basin near Drangajökull indicated 30-40%  
10 underestimate of precipitation, whereas the latter ( $p_2$ ) seems fairly representative for the  
11 measured runoff. Therefore  $p=p_2$  is used for the period 1991-2011 and  $p=kp_1$  for the period  
12 1960-1990, where  $k=P_2/P_1$  and  $P_2$  and  $P_1$  represent the total winter precipitation falling on the  
13 glacier in the years 1991-2006 (15 winters) integrated from  $p_2$  and  $p_1$ , respectively. This results  
14 in  $k=1.30$ . If the period is split into the first 8 and last 7 winters, ratios of 1.34 and 1.26 are  
15 obtained, indicating rather low variability on decadal time scales.

16 From Eq. 4-6 a scaled degree-day factor  $ddf=5.4 \text{ mm } ^\circ\text{C}^{-1}$  was obtained. The  $ddf$ s calculated by  
17 using other periods for scaling are quite consistent. For the periods, 1960-1975, 1975-1985,  
18 1985-1994 and 1994-2005 we get  $ddf$  in the range  $5.1-5.7 \text{ mm } ^\circ\text{C}^{-1}$  with  $0.28 \text{ mm } ^\circ\text{C}^{-1}$  standard  
19 deviation. To derive a cautious estimate of the uncertainty in the seasonal correction we assume  
20 the variability in  $ddf$  is not due to errors in estimated winter precipitation or errors in the deduced  
21 volume change but due to Gaussian noise caused by the variability in the degree-day factor  
22 relating the temperature record and the actual ablation. The standard deviation of  $ddf$  for  
23 individual years can be formulated as  $\sim\sqrt{11} \cdot 0.28 \text{ mm } ^\circ\text{C}^{-1}$  (11 years is the average length of  
24 the periods). This multiplied by 1.96 (assuming normal distribution) gives us the 95%  
25 confidence level and therefore  $ddf=5.4 \pm 1.8 \text{ mm } ^\circ\text{C}^{-1}$ . Assuming that our conversion factor  
26  $c_{\Delta V_{\text{ice}}/\Delta T_{\text{ice}}}=0.75 \pm 0.1$  (where  $c_{\Delta V_{\text{ice}}/\Delta T_{\text{ice}}}=0.65$  corresponds volume change mostly due to melting of  
27 snow and  $c_{\Delta V_{\text{ice}}/\Delta T_{\text{ice}}}=0.85$  corresponds to volume change mostly due melting of ice) is  
28 independent of  $ddf$ , results in seasonal corrections from Eq. 3 with 37% uncertainty (95%  
29 confidence level). The seasonal volume correction of each DEM is shown in Table 3.

30 The interpolated temperature grids were not available for 2011. Therefore the seasonal  
31 correction of the 2011 DEM was instead based on the average daily temperatures at 2 m height  
32 above ground in a 3 km x 3 km grid, extracted from the RÁV dataset (Rögnvaldsson et al.,  
33 2011), which was prepared by dynamically downscaling the operational analysis of the

1 ~~ECMWF with the A-WRF mesoscale atmospheric model (Skamarock et al. 2008). The degree~~  
2 ~~day factor was scaled specifically for these temperature grids, using the period between the~~  
3 ~~DEMs in 2005 and 2011 and the same procedure as described above using the interpolated~~  
4 ~~precipitation maps (Crochet, 2013). The assumed uncertainty in the 2011 seasonal correction~~  
5 ~~corresponds to 37% of the total correction. The aerial photographs used to produce the 1946~~  
6 ~~DEM were taken at the beginning of October before the start of winter snow fall. No seasonal~~  
7 ~~correction was therefore required.~~ Published values of  $ddf$  for Langjökull, Hofsjökull and  
8 Vatnajökull ice caps in Iceland (Jóhannesson et al., 2007; Guðmundsson et al., 2009) using  
9 comparable temperature data spans the range from 4.45 mm w.e. °C<sup>-1</sup> (minimum value for snow  
10 using lapse rate of 0.56 °C km<sup>-1</sup>; Jóhannesson et al., 2007) to 7.5 mm w.e. °C<sup>-1</sup> (maximum value  
11 of firn/ice using lapse rate of 0.6 °C km<sup>-1</sup>; Guðmundsson et al., 2009). If these values had been  
12 obtained with -lapse rate equal to the one ~~used in~~ applied when creating the ~~for~~ temperature grids  
13 ~~used here (6.5°C km<sup>-1</sup>) the resulting  $ddf$  would have been slightly higher~~lower. We therefore  
14 ~~use  $ddf=6.5\pm 1.5$  mm w.e.°C<sup>-1</sup> instead of  $ddf=6.0 \pm 1.5$  mm w.e.°C<sup>-1</sup> (covering the span of~~  
15 ~~published values).~~ Assuming that our conversion factor  $c_{\delta V_{S,cor}}=0.75\pm 0.1$  (where  $c_{\delta V_{S,cor}}=0.65$   
16 ~~corresponds to volume change mostly due to melting of snow and  $c_{\delta V_{S,cor}}=0.85$  corresponds to~~  
17 ~~volume change mostly due melting of ice) is independent of  $ddf$ , results in seasonal corrections~~  
18 ~~from Eq. 3 with 2837% uncertainty (95% confidence level). The value of  $ddf$  is actually lower~~  
19 ~~for snow than firn/ice, hence this assumption should lead to overestimate of the ratio~~  
20  ~~$ddf/c_{\delta V_{S,cor}}$  and consequently the uncertainty range of  $\delta V_{S,cor}$  derived from Eq. 3. The~~  
21 ~~seasonal volume correction of each DEM is shown given in Table 3.~~

22 ~~The interpolated temperature grids were not available for 2011. Therefore the seasonal~~  
23 ~~correction of the 2011 DEM was instead based on the average daily temperatures at 2 m height~~  
24 ~~above ground in a 3 km x 3 km grid, extracted from the RÁV dataset (Rögnvaldsson et al.,~~  
25 ~~2011), which was prepared by dynamically downscaling the operational analysis of the~~  
26 ~~ECMWF with the A-WRF mesoscale atmospheric model (Skamarock et al. 2008). The degree~~  
27 ~~day factor was scaled specifically for these temperature grids, using the period between the~~  
28 ~~DEMs in 2005 and 2011 and the same procedure as described above using the interpolated~~  
29 ~~precipitation maps (Crochet, 2013). The assumed uncertainty in the 2011 seasonal correction~~  
30 ~~corresponds to 37% of the total correction.~~The aerial photographs used to produce the 1946  
31 DEM were taken at the beginning of October before the start of winter snow fall. No seasonal  
32 correction was therefore required.

## 2.7 Deriving the geodetic mass balance and its uncertainty

The glacier-wide mass balance rate,  $\dot{B}$  (the UNESCO, IACS mass balance terminology (Cogley et al., 2011) is adopted) is estimated during the period  $t_s - t_f$ , using the equation:

$$\dot{B}(t_s, t_f) = \frac{\delta V^*(t_s, t_f)}{\bar{A}(t_s, t_f) \cdot \delta t} c_{\delta V} \quad (74)$$

where  $\delta t = t_f - t_s$  and  $\bar{A}(t_s, t_f) = (A(t_s) + A(t_f))/2$  approximates the average area of the glacier during the period. It is reasonable to assume that the variables in Eq. 74 are independent of one another, hence the uncertainty in  $\dot{B}$  can be approximated as

$$\begin{aligned} \Delta \dot{B} &\approx \sqrt{\left(\Delta \delta V^* \frac{\partial \dot{B}}{\partial \delta V^*}\right)^2 + \left(\Delta \bar{A} \frac{\partial \dot{B}}{\partial \bar{A}}\right)^2 + \left(\Delta c_{\delta V} \frac{\partial \dot{B}}{\partial c_{\delta V}}\right)^2} \\ &= \frac{1}{\delta t} \sqrt{\left(\Delta \delta V^* \frac{c_{\delta V}}{\bar{A}}\right)^2 + \left(\Delta \bar{A} \frac{\delta V^* c_{\delta V}}{\bar{A}^2}\right)^2 + \left(\Delta c_{\delta V} \frac{\delta V^*}{\bar{A}}\right)^2} \quad (85) \end{aligned}$$

$\Delta \bar{A} = 4 \text{ km}^2$  is applied in all cases corresponding to  $\sim 2.5\%$  of the glacier area, which is considered a generous estimate of the uncertainty in the glacier area for the given definition (Sect. 2.4). We used  $c_{\delta V} = 0.85 \pm 0.06$  (Huss, 2013).

When estimating  $\Delta \delta V^*$  the error budget of  $\delta V^*$  was examined. The error,  $\varepsilon$ , of the seasonally corrected volume change,  $\delta V^*(t_s, t_f)$ , is the sum:

$$\begin{aligned} \varepsilon\{\delta V^*(t_s, t_f)\} &= \varepsilon\{V_m(t_s)\} + \varepsilon\{V_i(t_s)\} + \varepsilon\{\delta V_{S\_cor}(t_s)\} + \\ &\varepsilon\{V_m(t_f)\} + \varepsilon\{V_i(t_f)\} + \varepsilon\{\delta V_{S\_cor}(t_f)\} \quad (96) \end{aligned}$$

where the error in the measured volume at time  $t$  is

$$\varepsilon\{V_m(t)\} = A_m(t) \cdot \bar{\varepsilon}\{h(t)\} \quad (107)$$

1 where  $A_m$  is the area of measured DEM within the glacier and  $\bar{\varepsilon}\{h\}$  the mean error of the  
 2 glaciated area. The error in volume for the interpolated glacier sections lacking measurement  
 3 (Sect. 2.3) is

$$\varepsilon\{V_i(t)\} = \sum_{j=1}^N A_j(t) \cdot \bar{\varepsilon}\{h_j(t)\} \quad (118)$$

6  
 7 where  $A_j$  is the area of the interpolated section,  $j$ , and  $\bar{\varepsilon}\{h_j\}$  is the corresponding mean elevation  
 8 error. Assuming that the individual errors contributing to Eq. 9-6 and 8-11 are independent of  
 9 one another the probability function of the error in  $\delta V^*(t_s, t_f)$  is given by the multiple  
 10 convolutions:

$$f_{\varepsilon\{\delta V^*(t_s, t_f)\}} = f_{\varepsilon\{V_m(t_s)\}} * f_{\varepsilon\{V_i(t_s)\}} * f_{\varepsilon\{\delta V_{s,cor}(t_s)\}} * f_{\varepsilon\{V_m(t_f)\}} * f_{\varepsilon\{V_i(t_f)\}} * f_{\varepsilon\{\delta V_{s,cor}(t_f)\}} \quad (9)$$

13  
 14 The probability function  $f_{\varepsilon\{V_m(t)\}}$  was derived directly from Eq. 10 and by approximating  
 15  $f_{\bar{\varepsilon}\{h(t)\}}$  using the histogram of the corresponding elevation bias correction (Sect. 2.2) minus its  
 16 mean. All other errors are assumed to be normally distributed with zero mean, hence

$$f(\varepsilon) = \frac{1}{\sigma_\varepsilon \sqrt{2\pi}} e^{-\frac{\varepsilon^2}{2\sigma_\varepsilon^2}} \quad (130)$$

19  
 20 The probability distribution  $f_{\varepsilon\{V_i\}}$  is hence also a normal distribution with

$$\sigma_{\varepsilon\{V_i\}} = \sqrt{\sum_{j=1}^N (A_j \cdot \sigma_{\bar{\varepsilon}\{h_j\}})^2} \quad (141)$$

23  
 24 The uncertainty in the volume change  $\Delta\delta V$  (95% confidence level) was now derived from the  
 25 probability distribution given by Eq. 129. Table 3 shows the 95% confidence level of  $f_{\varepsilon\{V_m\}}$ ,  
 26  $f_{\varepsilon\{V_i\}}$  and  $f_{\varepsilon\{\delta V_{s,cor}\}}$  for each year of acquisition, revealing the main source of error in the  
 27 derived volume changes.

1

## 2 **3 Results**

### 3 **3.1 Bias corrections and uncertainty estimates deduced from the DEM errors**

4 Table 2 gives values of several error estimation parameters for the photogrammetric DEMs  
5 deduced by comparison with the 2011 LiDAR DEM in ice and snow free areas. Some of these  
6 parameters can be used both to correct the DEMs and to estimate the uncertainty of geodetic  
7 mass balance results. In some cases significant difference is observed between the mean DEM  
8 error, commonly used to correct for bias (0 order correction) of the DEM (e.g. Guðmundsson  
9 et al. 2011), and the bias derived from the SGSim. The greatest difference is for the 1946 DEM,  
10 which after removal of outliers and steep slopes the ice and snow free part of it has a mean error  
11 of -0.86 m whereas the SGSim results in bias of 1.66 m. The difference would presumably be  
12 lower if we would only calculate the mean error using areas within certain distance from the  
13 glacier margin but it is not straight forward to select this distance without using geostatistical  
14 approaches.

15 The parameters in Table 2 that can be used to estimate the uncertainty of geodetic mass balance  
16 show even more diversity. The crudest parameter would be the standard deviation of the DEM  
17 error derived from ice and snow free areas. Standard deviation is commonly interpreted as 68%  
18 confidence level assuming normal error distribution and should therefore be multiplied by 1.96  
19 to obtain 95% confidence level as derived for the other two approaches shown in Table 2. This  
20 interpretation of the standard deviation as uncertainty proxy of the volume change implies the  
21 assumption that the DEM errors at different locations within the glacier are totally correlated  
22 (Rolstad et al., 2009). Since the confidence level of geodetic mass balance results is typically  
23 not mentioned in studies using the standard deviation as their uncertainty proxy, the conversion  
24 of the standard deviation to 95% confidence level is omitted in Table 2. The values of standard  
25 deviation for the ice free DEMs are 5-45% lower after removal of outlier and steep slopes. The  
26 lower standard deviation values are however still by far higher than the uncertainty (95% conf.  
27 level) of the bias correction derived with SGSim. The SGSim results in uncertainty between  
28 0.21 m (in 2005) and 1.58 m (in 1946). The SGSim uncertainties correspond to 24-46% of the  
29 standard deviation (after slope and outlier removal). If we exclude the three DEMs from 1960,  
30 covering only ~1/3 of Drangajökull each, the range is 24-33%. The SGSim uncertainties  
31 correspond to 27-80% of the uncertainties derived with method described by Rolstad et al.  
32 (2009) and the percentage seems to depend strongly on the range of the spherical semivariogram  
33 model used in both calculations (Fig. 8).

### 3.2 DEM seasonal corrections and contribution of different error sources to the geodetic mass balance

The effects of seasonal correction and the estimated contribution of each type of error to the total volume change is summarised in Table 3. The importance of seasonal correction for Drangajökull is clearly revealed, particularly for the first two periods, 1946-1960 and 1960-1975, due to the early acquisition of the 1960 aerial photographs. The sum of the two seasonal corrections for these periods corresponds to larger value than the derived total uncertainty of  $\delta V^*$ . The correction effectively increases the difference in  $\dot{B}$  between the periods by 0.4235 m w.e. a<sup>-1</sup> (~0.17-21 m w.e. a<sup>-1</sup> absolute change for each period). With the inferred correction the period 1946-1960 is the period of highest mass loss rate, along with 1994-2005, whereas the period 1960-1975, is only slightly but still differs insignificantly from equilibrium negative (Fig. 9). For other periods the net seasonal correction changed the derived  $\dot{B}$  by 0.065-0.1208 m w.e. a<sup>-1</sup>.

The main source of uncertainties is different from one period to another, but in no case is the highest contribution is from the estimated uncertainty of the DEM elevation ( $\Delta\delta h_m$  in Table 3). For periods, where volume change is based on the 1946 or 1994 DEM, we have relative high uncertainties due to interpolations of large gaps in the derived DEMs (Fig. 3 and Table 2). The derived value of  $\delta V^*$  for the period 2005-2011, obtained from the best two DEMs in terms of accuracy and coverage, has significant uncertainty due large seasonal correction for both DEMs. The 2005 and 2011 data were acquired in late July, and the summer remainder for both years was relatively warm. The sum of seasonal corrections (which have opposite signs) is actually only half of the smaller than the uncertainty related to the seasonal corrections for the period 2005-2011.

The uncertainty percentage of  $\delta V^*$  is typically significantly higher than the uncertainty percentage of A (2.5%) and  $c_{\delta V}$  (~7%). Uncertainty of the derived  $\dot{B}$  (Fig. 9) produced by the uncertainty of the latter two variables is therefore generally minor compared to the uncertainty contribution of  $\delta V^*$ .

### 3.3 The geodetic mass balance of Drangajökull

Figure 9 shows the derived  $\dot{B}$  for Drangajökull during six intervals since 1946. During the period 1946-1960 relatively high mass loss rates of  $\dot{B} = -0.663 \pm 0.178$  m w.e. a<sup>-1</sup> are estimated. The mass balance rate was glacier was near equilibrium in much less negative in 1960-19875 with  $\dot{B} = -0.0710 \pm 0.078$  m w.e. a<sup>-1</sup> and and was then slightly (but statistically

1 ~~significant) positive in 1975–1994;  $\dot{B} = 0.079 \pm 0.088$  m w.e. a<sup>-1</sup> in 1960–1975 and 1975–1985,~~  
2 ~~respectively. The mass balance became significantly positive in 1985–1994 with  $\dot{B} =$~~   
3  ~~$0.26 \pm 0.11$  m w.e. a<sup>-1</sup> in 1975–1985 and 1985–1994, respectively.~~ In the period 1994–2005  
4 again, as in the mid-century, there is high rate of mass loss with  $\dot{B} = -0.643 \pm 0.10$  m w.e. a<sup>-1</sup>  
5 and then slightly less negative mass balance rate in 2005–2011, with  $\dot{B} = -0.460 \pm 0.154$  m  
6 w.e. a<sup>-1</sup>. The glacier wide mass balance rate for the entire period 1946–2011 is  $\dot{B} = -0.2658 \pm$   
7  $0.040$  m w.e. a<sup>-1</sup>. In the same period Drangajökull was reduced in area by ~11% from 161 km<sup>2</sup>  
8 to 144 km<sup>2</sup> (Fig. 8).

9 The two lower panels of Fig. 9 show  $\dot{B}$  for the western and eastern half of Drangajökull ice cap,  
10 as defined by the ice divides from north to south shown in Fig. 6. The results are derived in the  
11 same manner as the result for the entire glacier, where the steps taken to correct for bias of the  
12 DEM, derive seasonal correction and derive uncertainties were carried out focusing specifically  
13 on either the western or the eastern part. The bias correction of each half may vary up to few  
14 decimetres from the correction of the entire ice cap and the uncertainty limits of the bias  
15 correction is generally slightly higher. ~~By focusing the calculation on each half specifically we~~  
16 ~~also obtain different  $ddf$  for the seasonal correction. Assuming the same level of uncertainty as~~  
17 ~~when studying the entire ice cap we derive  $ddf=4.9\pm1.6$  mm °C<sup>-1</sup> and  $ddf=6.3\pm2.1$  mm °C<sup>-1</sup> for~~  
18 ~~the western and eastern part of Drangajökull, respectively, compared to  $ddf=5.4\pm1.8$  mm °C<sup>-1</sup>~~  
19 ~~for the entire ice cap.~~

20 Figure 9 shows different evolution of the west and east glacier. Both parts suffered significantly  
21 negative mass balance rate in 1946–1960 and 1994–2011. The period in between was  
22 significantly negative on the east side, apart from the period ~~1985–1994–2005~~, when the upper  
23 95% confidence level is slightly above 0, whereas the western part had  $\dot{B}$  near 0 in 1960–1975  
24 and significantly positive mass balance rate with  $\dot{B} = 0.235 \pm 0.10$  m w.e. a<sup>-1</sup> and  $\dot{B} =$   
25  $0.520 \pm 0.15$  m w.e. a<sup>-1</sup> in 1975–1985 and 1985–1994, respectively. ~~Mean  $\dot{B}$~~  mass balance rate  
26 of  $\dot{B} = -0.158636 \pm 0.0520$  m w.e. a<sup>-1</sup> is estimated for the period 1946–2011 on the western  
27 part. The mass loss rate is on average ~3-fold higher for the eastern part with  $\dot{B} =$   
28  $-0.4106376 \pm 0.04396$  m w.e. a<sup>-1</sup>. This is also reflected in the area change but in 1946–2011  
29 the eastern part decreased in area 21%, while the western part shrank only by 3% (Fig. 8).

### 30 ~~3.4 ——— Modelled annual SMB~~

31 ~~The method described for deriving the seasonal correction of the volume change results in a~~  
32 ~~routine for estimating  $\dot{B}_w$ ,  $\dot{B}_e$  and  $\dot{B}$  on annual bases using the derived  $ddf$ s and Eq. 5–6 modified~~

1 by using time span corresponding to each glaciological year back to 1958 (Fig. 10a;  $\dot{B}_g$  extends  
2 back to 1949). To validate how this simple model works for deriving  $B$  we compare the  
3 modelled mass balance rate,  $\dot{B}_{mod}$ , for each period since 1960, with the derived geodetic results  
4 for the same periods (Fig. 9). When looking at the entire ice cap  $\dot{B}_{mod}$  (calculated without  
5 uncertainties) is within the 95% confidence limit in 3 of 5 cases but slightly outside the limits  
6 in two periods. This indicates a reasonable fit when considering the simplicity of the model.  
7  $\dot{B}_{mod}$  obtained for the western and eastern halves of the glacier with the specifically scaled *ddf*s  
8 (Sect. 3.3) is also shown in Fig. 9 for all periods since 1960.  $\dot{B}_{mod}$  is generally outside (3 out  
9 of 5) or near the 95% limits of the geodetic results for the western part of the glacier, while on  
10 the eastern part  $\dot{B}_{mod}$  is within the 95% confidence level in 4 of the 5 periods.

11 The model results on annual bases for the entire glacier (Fig. 10a) indicates  $\dot{B}_w$  generally  
12 varying between 2 and 3 m w.e. a<sup>-1</sup> in 1958 to 2011,  $\dot{B}_s$  between -2 and -4 m w.e. a<sup>-1</sup> and  $\dot{B}$   
13 ranging from -1.9 and 1.4 m w.e. a<sup>-1</sup>. The model shows that the highest value of  $\dot{B}$  observed in  
14 1985-1994 period is partly due to unusually positive mass balance for the glaciological year  
15 1991-92 and 1992-93, when winters of relatively high accumulation were followed by rather  
16 cold summers. In 1994-2011 when the geodetic data shows relatively high mass loss rate the  
17 annual  $\dot{B}$  was probably often near zero or even positive. Most of the mass loss probably  
18 occurred during the glaciological years 2002-03, 2003-04 and 2009-10 that according to the  
19 model are listed in place 1-3 in terms of negative mass balance for the period 1958-2011.

## 21 4 Discussion

22 The high precision of the geodetic mass balance results presented can be primarily explained  
23 by: i) The use of the high resolution and accuracy LiDAR DEM to extract evenly distributed  
24 GCPs for constraining the orientation of photogrammetric DEMs; obtaining equivalent  
25 distribution of GCPs in the field was not possible within the financial frame of this study. ii)  
26 The thorough uncertainty assessment of the results where the LiDAR data from ice and snow  
27 free areas is also a key data since it enables assessment of geo-statistical parameters of the  
28 photogrammetric DEMs. Both i and ii, highlight the need of high resolution and accuracy DEMs  
29 from the present in areas of interest to conduct studies of geodetic mass balance using aerial  
30 photographs from the past. The third important use of the LiDAR data in this study, is the  
31 creation of DEMs from the photogrammetric point clouds within the glacier. Rather than  
32 interpolating the elevation point clouds directly we interpolate the difference between the point

1 cloud and LiDAR DEM (much less high frequency variability, the difference is a smoother  
2 surface ~~as pointed out by (Cox and March, (2004))~~ and add the interpolated product to the  
3 LiDAR DEM. This results in more accurate DEMs in areas where the density of the  
4 photogrammetric point clouds is low.

5 Other state of the art high resolution elevation data sets obtained with airborne or spaceborne  
6 sensors are also suitable to replace the LiDAR data in the work procedure described here. This  
7 probably includes Worldview and Pléiades high resolution stereo images, allowing extraction  
8 of DEM with <5m cell dimensions and orthorectified photographs with <1mx 1m cell size (e.g.  
9 Berthier et al., 2014; Howat et al., 2015). Part of the work procedure described has already been  
10 carried out using such satellite data as replacement for the airborne LIDAR. I-but in a recent  
11 study by Papasodoro et al. (2015), Pléiades data was used to collect GCPs for constraining  
12 DEMs from aerial photographs. Even though the absolute accuracy of data from spaceborne  
13 sensors does not match data from airborne LiDAR, it does not make the satellite data  
14 inadequate. Each photogrammetric DEM from the past is-can be fixed into the reference frame  
15 of the high resolution DEM through the extraction and usage of GCPs and implementation of  
16 proposed bias correction. The relative elevation change between DEMs should therefore be  
17 fairly accurate despite lower absolute accuracy of the DEMs, and shifts and tilts of the reference  
18 frame cancels out in DEM differencing.

19 In this study, the derived bias correction of the glaciated DEM section and the uncertainty of  
20 volume changes related to DEM errors are obtained from the probability distribution calculated  
21 by using SGSim. The bias correction corresponds to the probabilistic mean of the average error  
22 within the glacier. As shown in Table 2 the difference between the mean error in snow and ice  
23 free areas and the bias derived from the SGSim (the estimated probabilistic mean of the glacier  
24 DEM error) was up to 2.5 m (in 1946). This difference would presumably be lower if we would  
25 only calculate the mean error using areas within certain distance from the glacier margin but it  
26 is not straight forward to select this distance without using some geo-statistical approaches. The  
27 relation is also not obvious between the probabilistic mean of an average DEM error within the  
28 glacier and higher order corrections of a glacier DEM obtained with least square fit (or similar)  
29 using deduced DEM errors in ice and snow free areas. If the average correction does not  
30 correspond to the probabilistic mean, the results of geodetic mass balance will be incorrectly  
31 centered even if the width of the error bars is realistic.

32 When comparing different proxies used for estimating the uncertainty of DEM difference  
33 derived volume change, it is no surprise that using the standard deviation of the DEM error in

1 snow and ice free areas leads to great overestimate of the uncertainty (Table 2). This has been  
2 shown before by Rolstad et al. (2009). Other estimators that ignore information of the spatial  
3 dependency of the DEM errors, such as the NMAD value (Höhle and Höhle, 2009), should also  
4 be considered as incomplete for this purpose.

5 The difference in uncertainty estimates between the method described here and the method of  
6 Rolstad et al. (2009) is especially noteworthy (Table 2 and Fig. 8). Rolstad et al. (2009)  
7 provided a simple and logical method to estimate the uncertainty of derived volume change.

8 The DEM errors (or difference) in ice and snow free areas are used to calculate a ~~\_semi-~~  
9 semivariogram that constrains a spherical semivariogram model. From the spherical  
10 semivariogram model alone the expected variance of the DEM error ( $\sigma_{z_{bias}}^2$ ) averaged over  
11 circular region corresponding to the size of the glacier is calculated analytically. The method  
12 compensate for the spatial dependency of the DEM error at different location within the glacier.  
13 The method does however not take into the account how the DEM error within the glacier  
14 depends on the DEM errors outside the glacier, unlike the method proposed here utilizing  
15 SGSim. This is most likely the explanation why the ratio between the two uncertainty estimates  
16 ( $\Delta z_{biasSGSim}/\Delta z_{biasRols.}$ ) appears to be strongly dependent on the range,  $r$ , in the spherical  
17 semivariogram model, which is common for both approaches (Fig. 8). If  $r$  is small compared  
18 the size of the glacier, meaning that large proportion of the glacier has DEM error independent  
19 of DEM error outside the glacier, the uncertainty derived SGSim is only slightly smaller than  
20 the uncertainty derived analytically from the spherical semivariogram model alone. If  $r$  is  
21 however large, meaning that large proportion or even the entire glacier has DEM error  
22 dependent on the DEM errors outside the glacier, the SGSim results in much lower uncertainty.  
23 This interpretation implies that the method of Rolstad et al. (2009) gives a good approximation  
24 of the uncertainty if most of the glaciated area is at distance  $>r$  from ice and snow free areas  
25 providing measurements of the DEM errors, but can otherwise result in great overestimate of  
26 the uncertainty in the derived volume change. The main disadvantage of SGSim approach  
27 compared to the approach of Rolstad et al. (2009) is that is more time consuming. The tool  
28 applied here (WinGSlib) also has problems with dataset larger than worked with in this study.  
29 New tools enabling the SGSim approach for large data sets should however be developed in  
30 order to facilitate the usage of this methodology.

31 Our study emphasises the importance of including seasonal correction of DEMs for glacier with  
32 high mass turnover to avoid wrong interpretation of derived volume change. The most extreme  
33 case is the negative volume change derived from the difference between the 1960 and 1975

1 DEMs. The seasonal correction results in  $\sim 23/43$  of the of this negative volume change being  
2 effectively transferred in to the period 1946-1960 due to large seasonal correction of the 1960  
3 DEM resulting from relatively early acquisition of the aerial photographs (Table 1). The  
4 seasonally corrected volume change revealing the volume change between the start of different  
5 glaciological year obviously has higher uncertainty than the uncorrected volume change. We  
6 however consider this trade-off important for easy comparison with other data records,  
7 including meteorological data and in situ mass balance measurements. The uncertainty due to  
8 the seasonal correction as well as the uncertainty related to the interpolation of the data gaps  
9 should be considered as cautious estimates of the 95% confidence level of the error associated  
10 with these two error sources. Effort should be made to constrain these uncertainties further,  
11 which could narrow the uncertainty estimates of this study and other similar even further, but  
12 it is beyond the scope of this paper.

13 The presented geodetic mass balance record indicate slower volume decrease for Drangajökull  
14 ice cap since the 1940's than for most other glacier in Iceland with geodetic mass balance record  
15 extending back to that period. While we observe  $\dot{B} = -0.25860 \pm 0.040$  m w.e. a<sup>-1</sup> for  
16 Drangajökull in the period 1946-2011 the corresponding values for Langjökull ice cap in 1945-  
17 2011 is  $\dot{B} \approx -0.5$  m w.e. a<sup>-1</sup> (Fig. 10e Pálsson et al., 2012, with extension from traditional mass  
18 measurements in 2004-2011 from; Björnsson et al., (2013) until 2010,; and -unpublished  
19 Institute of Earth Sciences (IES) IES data for 2011-reference?). Two outlets of S-Vatnajökull,  
20 Kvíárjökull and Skaftárjökull have similar rate of mass decrease in 1945-2010 or  $\dot{B} \approx -0.25$   
21 m w.e. a<sup>-1</sup> (Hannesdóttir et al., 2015). Other outlets of S-Vatnajökull ice cap show  $\bar{B}_n$  between  
22 -0.3 and -0.8 m w.e. a<sup>-1</sup> in 1945-2010 (Hannesdóttir et al., 2015; Aðalgeirsdóttir et al., 2011).  
23 For the relatively warm period in 1994-2011 we obtain  $\dot{B} = -0.5852 \pm 0.0874$  m w.e. a<sup>-1</sup>,  
24 which is in good agreement with the study of Jóhannesson et al. (2013), which indicated  $\dot{B} \approx$   
25  $-0.5$  m w.e. a<sup>-1</sup> for Drangajökull ice cap in the period 1996-2011. Comparison of Drangajökull  
26 mass balance in 1994-2011, with results from traditional in situ mass balance measurements  
27 from Langjökull (in 1996-2011) and Vatnajökull ice caps (Fig. 10a) show that the reduction  
28 rate has been  $\sim 1450\%$  faster on Langjökull ( $\dot{B} \approx -1.4$  m w.e. a<sup>-1</sup>, from Björnsson et al., (2013)  
29 until 2010, and -unpublished IES IES -data-reference??) for 2011) and  $\sim 230\%$  faster on  
30 Vatnajökull ( $\dot{B} \approx -0.7$  m w.e. a<sup>-1</sup>, from Björnsson et al., (2013) until 2010, and unpublished  
31 IES IES data for 2011-reference??).

32 The difference in the geodetic mass balance results between the east and west part of  
33 Drangajökull highlights how difficult it is to extrapolate mass balance records from one glacier

1 to another, even over short distances. The results, showing ~3 times more negative mass balance  
2 rate for the eastern part of Drangajökull than the western part for the entire period 1946-2011,  
3 is not reflected in changing spatial trends of summer temperature during the period. The  
4 summer temperature measured east of Drangajökull is typically ~1°C lower than revealed by  
5 measurements west of Drangajökull (Fig. 9.10c) and this is rather consistent throughout the  
6 survey period. Daily precipitation maps (1 km x 1 km cell size) in 1958-2006 deduced from  
7 ERA-40 (Uppala, 2005) by dynamic downscaling with linear model of orographic precipitation  
8 (an update of Crochet et al. (2007) described in Jóhannesson et al. (2007))The precipitation  
9 maps do not indicate strong trend in winter accumulation-precipitation from east to west. The  
10 fact that we obtain good fit between geodetic and modelled mass balance records for the eastern  
11 part of the ice cap with relatively high  $ddf$  but much worse fit for the western part with relatively  
12 low  $ddf$  could be an indication of an underestimated winter accumulation for western  
13 Drangajökull. The modelled winter precipitation may however not be representative for winter  
14 accumulation explanation for this may be due to excess of lee-drying in the by the LT-  
15 modelled precipitation or transport of snow from east to west by snow drift but; the most  
16 common wind direction on Drangajökull is from NE. Most of the precipitation also falls on the  
17 glacier when the wind blows from NE. Ongoing geodetic mass balance studies of Drangajökull  
18 on seasonal time scale may reveal further answers.

19 The modelled mass balance record of Drangajökull show annual mass turnover of ~2.5 m w.e.,  
20 significantly higher than at both Vatnajökull and Langjökull ice caps (Fig. 10). If the winter  
21 accumulation for western part of Drangajökull is underestimated causing underestimate for the  
22 entire ice cap by a factor of 5.4/6.3 (like the difference between  $ddf$  for the entire glacier and  
23 on the east side might suggest) the annual mass turnover is even higher or ~3 m w.e. The  
24 modelled record of Drangajökull indicates that the difference in typical year for the positive  
25 and negative periods is actually not so great. The difference in the median of annual  $\dot{B}_s$  for the  
26 negative period 1975-1994 and the positive period 1994-2011 is only ~0.2 m w.e. a<sup>-1</sup>. The main  
27 difference between the periods is however caused by few years of extreme mass balance with  
28 opposite signs. Figure 10a reveals striking similarities between the modelled  $\dot{B}_s$  on  
29 Drangajökull and the  $\dot{B}_s$  derived with traditional mass balance measurements on Langjökull ice  
30 cap, except for the last two years when  $\dot{B}_s$  on Langjökull was enhanced by ash fall from the  
31 2010 Eyjafjallajökull eruption and 2011 Grímsvötn eruption.  $\dot{B}_s$  on Drangajökull and  
32 Langjökull does however correlate much worse with measured on Vatnajökull.

1 The geodetic mass balance record on Drangajökull ice cap is the first such record revealing  
2 glacier volume change in Iceland on decadal time scale the past ~70 years. Other records  
3 spanning this period have coarser resolution particularly ~~over~~ the period 1945-1985, which is  
4 typically assigned a single mass balance value (~~Fig. 10~~e.g. Pálsson et al., 2012; Hannesdóttir  
5 et al., 2015). However, accurate and detailed studies pertaining to this period are of particular  
6 interest as they may reveal how the Icelandic glaciers responded to the change from a relatively  
7 warm climate in 1925-1965 to a significantly colder climate in 1965-1990, and subsequently to  
8 a warming with a short setback around 1995 (cf. Figs 2.6 and 3.1 in Björnsson et al., 2008). We  
9 consider this study the first step in filling this gap in our knowledge. The key data to continue  
10 this work is the archive of aerial photographs at the National Land Survey of Iceland, covering  
11 the Icelandic glaciers in the 1940's-1990's. Similar archives covering other glaciated parts of  
12 the world should be fully utilized using the new processing techniques and recent and future  
13 availability ~~the~~ of high resolution DEMs of the present state of the glaciated areas and its  
14 vicinity.

## 16 5 Conclusions

17 This paper highlights the opportunities that new high resolution DEMs are opening to improve  
18 the procedure carried out to obtain geodetic mass balance records. Such DEMs is aare key data  
19 in three aspects of this study: a) Extracting GCPs from . We demonstrated how we combine  
20 aerial photographs with recent airborne LiDAR ~~data-DEM~~to to constrain photogrammetric  
21 extract DEMs at 6 different epochs-at 6 different epochs in 1946-2005. b) Interpolate over  
22 glacier surface the elevation difference of derived photogrammetric point cloud relative to the  
23 LiDAR DEM. -without any additional support from field data.-

24 ~~We describe a geostatistical method, using the LiDAR data~~c) Apply new geostatistical,  
25 approach based on comparison with the LiDAR data, to estimate simultaneously a bias  
26 correction for the glacier DEMs along with its 95% confidence level. The latter reveals the  
27 uncertainty associated with DEM errors in geodetic mass balance record.

28 The new geostatistical method applies SGSims using the DEM errors in ice and snow free areas  
29 and a spherical semivariogram model constrained by the DEM errors as input data. The  
30 resulting bias correction may differ considerably (in our case up to 2.5m in 1946) from the  
31 simple approach of applying bias correction using the mean DEM error outside the glacier. The  
32 resulting uncertainty of the DEM (95% conf. level) was typically estimated 20-35% of the  
33 standard deviation derived from the DEM errors in ice and snow free areas after outliers and

1 high slopes were masked out. The uncertainty contribution from DEM errors obtained with  
2 SGSim was 25-80% of the uncertainty estimate obtained with the geostatistical method of  
3 Rolstad et al. (2009). ~~The percentage decreases with the range, r, in the spherical variogram~~  
4 ~~model, which is common in both methods and measures the maximum distance over which~~  
5 ~~DEM errors are dependent.~~ We argue that methods typically carried out in uncertainty  
6 assessments of geodetic mass balance generally overestimate the uncertainty related to DEM  
7 errors, while the geostatistical approach described here results in more realistic uncertainty  
8 estimates.

9 This study also reveals the importance of seasonal corrections of geodetic mass balance for  
10 glaciers with high annual turnover; Drangajökull is a good example. The highest correction in  
11 our study was  $-3.5$  m (in 1960), which corresponds to  $\sim 32/43$  of the average elevation change  
12 between the 1960 and the 1975 DEMs.

13 During the whole period 1946-2011 we obtain  $\dot{B} = -0.2658 \pm 0.040$  m w.e.  $a^{-1}$  for entire  
14 Drangajökull. This is among the lowest retreat rate reported for glaciers in Iceland spanning  
15 approximately this period. Only two outlet glaciers in S-Vatnajökull have been reported with  
16 similar retreat rate. When calculating this for the western and eastern half of Drangajökull  
17 specifically we obtain  $\dot{B} = -0.158636 \pm 0.0520$  m w.e.  $a^{-1}$  and  $\dot{B} = -0.4061376 \pm$   
18  $0.03946$  m w.e.  $a^{-1}$ , respectively. This difference between east and west part of the glacier  
19 varies significantly during the survey period and does not seem to be related to relative changes  
20 in summer temperature. This great difference between east and west shows how difficult it is  
21 to extrapolate mass balance record from one glacier to another even over short distances. No  
22 glacier unit in Iceland has been reported as close to equilibrium on average since the 1940's as  
23 the western part of Drangajökull ice cap.

## 24 25 **Authors contributions**

26 The writing of this paper and the research it describes was mostly carried out by the first two  
27 authors of this paper, with inputs from the other three co-authors. All photogrammetric  
28 processing and revision of the resulting point clouds was carried out by J.M.C.B. The  
29 interpolation of the point cloud differences compared to the LiDAR DEM and construction of  
30 glacier DEM based on that, interpolation of data gaps, delineation of glacier margin, seasonal  
31 correction of the volume change, the construction of the presented mass balance records and  
32 associated error analysis was carried out by E.M. based on fruitful discussions with J.M.C.B.

1 and F.P. All figures in this paper were made by E.M. and J.M.C.B. as well as tables. P. C. and  
2 H. Á. contributed to the handling and interpretation of the meteorological data.

3

#### 4 **Acknowledgements**

5 This work was carried out within SVALI funded by the Nordic Top-level Research Initiative  
6 (TRI) and is SVALI publication number 70. It was also financially supported by alpS GmbH.  
7 This work is a contribution to the Rannís grant of excellence project, ANATILS. We thank the  
8 National Land Survey of Iceland and Loftmyndir ehf. for acquisition and scanning of the aerial  
9 photographs. This study used the recent LiDAR mapping of the glaciers in Iceland that was  
10 funded by the Icelandic Research Fund, the Landsvirkjun Research Fund, the Icelandic Road  
11 Administration, the Reykjavík Energy Environmental and Energy Research Fund, the Klima-  
12 og Luftgruppen (KoL) research fund of the Nordic Council of Ministers, the Vatnajökull  
13 National Park, the organization Friends of Vatnajökull, the National Land Survey of Iceland  
14 and the Icelandic Meteorological Office. We thank Cristopher Nuth and an anonymous  
15 reviewer for constructive reviews, as well as Etienne Berthier for helpful comments on the  
16 manuscript. We thank Alexander H. Jarosch ~~for~~ for fruitful discussion on the subject of this  
17 paper. Auður Agla Óladóttir is thanked for introducing the tools and methodology used in the  
18 error analysis of this study to E.M.

19

#### 20 **References**

- 21 Aðalgeirsdóttir, G., Guðmundsson, S., Björnsson, H., Pálsson, F., Jóhannesson, T.,  
22 Hannesdóttir, H., Sigurðsson, S. Þ. and Berthier, E.: Modelling the 20th and 21st century  
23 evolution of Hoffellsjökull glacier, SE-Vatnajökull, Iceland, *The Cryosphere*, 5(4), 961–975,  
24 doi:10.5194/tc-5-961-2011, 2011.
- 25 Barrand, N. E., Murray, T., James, T. D., Barr, S. L. and Mills, J. P.: Optimizing  
26 photogrammetric DEMs for glacier volume change assessment using laser-scanning derived  
27 ground-control points, *J. Glaciol.*, 55(189), 106–116, 2009.
- 28 Bauer, H., and Müller, J.: Height accuracy of blocks and bundle block adjustment with  
29 additional parameters, ISPRS 12th Congress, Ottawa, 1972.
- 30 Berthier, E., Schiefer, E., Clarke, G. K. C., Menounos, B. and Remy, F.: Contribution of  
31 Alaskan glaciers to sea-level rise derived from satellite imagery, *Nat. Geosci.*, 3(2), 92–95,  
32 doi:10.1038/ngeo737, 2010.

1 Berthier, E., Vincent, C., Magnússon, E., Gunnlaugsson, Á. Þ., Pitte, P., Le Meur, E., Masiokas,  
2 M., Ruiz, L., Pálsson, F., Belart, J. M. C. and Wagnon, P.: Glacier topography and elevation  
3 changes derived from Pléiades sub-meter stereo images, *The Cryosphere*, 8(6), 2275–2291,  
4 doi:10.5194/tc-8-2275-2014, 2014.

5 Björnsson, H., Sveinbjörnsdóttir, Á. E., Daníelsdóttir, A. K., Snorrason, Á., Sigurðsson, B. D.,  
6 Sveinbjörnsson, E. Viggósson, G., Sigurjónsson, J., Baldursson, S., Þorvaldsdóttir S. and  
7 Jónsson, T.: Hnattrænar loftslagsbreytingar og áhrif þeirra á Íslandi – Skýrsla vísindanefndar  
8 um loftslagsbreytingar. Umhverfissráðuneytið (The Icelandic Ministry for the Environment and  
9 Natural Resources), 118 pp, 2008.

10 Björnsson, H., Pálsson, F., Guðmundsson, S., Magnússon, E., Aðalgeirsdóttir, G., Jóhannesson,  
11 T., Berthier, E., Sigurðsson, O., and Thorsteinsson, T.: Contribution of Icelandic ice caps to sea  
12 level rise: trends and variability since the Little Ice Age, *Geophysical Research Letters*, 40, 1-  
13 5, doi: 10.1002/grl.50278, 2013.

14 ~~Björnsson, H., Pálsson, F., Guðmundsson M. T. and Haraldsson H. H.: Mass balance of western  
15 and northern Vatnajökull, Iceland, 1991–1995. *Jökull*, 45, 35–38, 1998.~~

16 Cardellini, C., Chiodini, G. and Frondini, F.: Application of stochastic simulation to CO<sub>2</sub> flux  
17 from soil: mapping and quantification of gas release, *J. Geophys. Res.*, 108(B9), ECV3–ECV1–  
18 13, 2003.

19 Clarke, G. K. C., Jarosch, A. H., Anslow, F. S., Radic, V. and Menounos, B.: Projected  
20 deglaciation of western Canada in the twenty-first century, *Nat. Geosci.*, 8(5), 372–377, 2015.

21 ~~Cogley, J. G.: Geodetic and direct mass-balance measurements: comparison and joint analysis,  
22 A. Glaciol., 50(50), 96-100, 2009.~~

23 Cogley, J. G., Hock, R., Rasmussen, L. A., Arendt, A. A., Bauder, A., Braithwaite, R. J.,  
24 Jansson, P., Kaser, G., Möller, M., Nicholson L. and Zemp, M.: Glossary of Glacier Mass  
25 Balance and Related Terms–, IHP-VII Technical Documents in Hydrology No. 86, IACS  
26 Contribution No. 2, UNESCO-IHP, Paris, 2011.

27 Cox, L. H. and March, R. S.: Comparison of geodetic and glaciological mass-balance  
28 techniques, Gulkana Glacier, Alaska, U. S. A., *J. Glaciol.*, 50(170), 363–370, 2004.

29 Crochet, P., Jóhannesson, T., Jónsson, T., Sigurðsson, O., Björnsson, H., Pálsson F., and  
30 Barstad I.: Estimating the spatial distribution of precipitation in Iceland using a linear model of  
31 orographic precipitation. *J. Hydrometeor.*, 8, 1285–1306, 2007.

- 1 Crochet, P. and Jóhannesson, T.: A dataset of daily temperature in Iceland for the period 1949–  
2 2010. *Jökull*, 61, 1–17, 2011.
- 3 ~~Crochet, P.: Gridding daily precipitation with an enhanced two-step spatial interpolation  
4 method. Tech. Rep.: PC/2013-01. Icelandic Meteorological Office. 26 pp, 2013.~~
- 5 Deutsch, C. V. and Journel, A. G.: *GSLIB. Geostatistical Software Library and User's Guide*,  
6 2nd ed. 369 pp. Oxford, New York: Oxford University Press. ISBN 0 19 510015 8, 1998.
- 7 Fischer, M., Huss, M. and Hoelzle, M.: Surface elevation and mass changes of all Swiss glaciers  
8 1980–2010, *The Cryosphere*, 9(2), 525–540, doi:10.5194/tc-9-525-2015, 2015.
- 9 Gardelle, J., Berthier, E., and Arnaud, Y.: Slight mass gain of Karakoram glaciers in the early  
10 twenty-first century, *Nat. Geosci.*, 5, 322–325, doi:10.1038/NGEO1450, 2012a.
- 11 Guðmundsson, S., Björnsson, H., Pálsson, F. and Haraldsson, H. H.: Comparison of energy and  
12 degree-day models of summer ablation on the Langjökull ice cap, SW-Iceland, *Jökull*(59), 1-  
13 18, 2009.
- 14 Guðmundsson, S., Björnsson, H., Magnússon, E., Berthier, E., Pálsson, F., Guðmundsson, M.  
15 T., Hognadóttir, T. and Dall, J.: Response of Eyjafjallajökull, Torfajökull and Tindfjallajökull  
16 ice caps in Iceland to regional warming, deduced by remote sensing, *Polar Res. Online*, 30,  
17 doi:10.3402/polar.v30i0.7282, 2011.
- 18 Hannesdóttir, H., Björnsson, H., Pálsson, F., Aðalgeirsdóttir, G. and Guðmundsson, S.:  
19 Changes in the southeast Vatnajökull ice cap, Iceland, between ~1890 and 2010. *The*  
20 *Cryosphere*, 9, 565–585, doi:10.5194/tc-9-565-2015, 2015.
- 21 Howat, I. M., Porter, C., Noh, M. J., Smith, B. E., and Jeong, S.: Brief Communication: Sudden  
22 drainage of a subglacial lake beneath the Greenland Ice Sheet, *The Cryosphere*, 9, 103-108,  
23 doi:10.5194/tc-9-103-2015, 2015.
- 24 Höhle, J. and Höhle, M.: Accuracy assessment of digital elevation models by means of robust  
25 statistical methods, *ISPRS J. Photogramm. Remote Sens.*, 64, 398–406,  
26 doi:10.1016/j.isprsjprs.2009.02.003, 2009.
- 27 Huss, M.: Density assumptions for converting geodetic glacier volume change to mass change,  
28 *The Cryosphere*, 7(3), 877–887, doi:10.5194/tc-7-877-2013, 2013.
- 29 Jacobsen, K.: Programmgesteuerte Auswahl der zusätzlicher Parameter, *Bildmessung und*  
30 *Luftbildwesen*, 213-217, 1982.

- 1 [James, T., Murray, T. Barrand, N. and Barr, S.: Extracting photogrammetric ground control](#)  
2 [from lidar DEMs for change detection, The Photogrammetric Record 21\(116\), 312-328, 2006.](#)
- 3 James, T. D., Murray, T., Barrand, N. E., Sykes, H. J., Fox, A. J. and King, M. A.: Observations  
4 of enhanced thinning in the upper reaches of Svalbard glaciers, *The Cryosphere*, 6(6), 1369–  
5 1381, doi:10.5194/tc-6-1369-2012, 2012.
- 6 Jóhannesson, T., Aðalgeirsdóttir, G., Björnsson, H., Crochet, P., Elíasson, E.B., Guðmundsson,  
7 S., Jónsdóttir, J.F., Ólafsson, H., Pálsson, F., Rögnvaldsson, Ó., Sigurðsson, O., Snorrason, Á.  
8 Sveinsson, Ó. G. B. and Thorsteinsson, T.: Effect of climate change on hydrology and hydro-  
9 resources in Iceland. Rep. OS-2007/011. National Energy Authority, 91 pp. 2007.
- 10 Jóhannesson, T., Björnsson, H., Pálsson, F., Sigurðsson, O., and Þorsteinsson, P.: LiDAR  
11 mapping of the Snæfellsjökull ice cap, western Iceland, *Jökull*, 61, 19–32, 2011.
- 12 Jóhannesson, T., Björnsson, H., Magnússon, E., Guðmundsson, S., Pálsson, F., Sigurðsson, O.,  
13 Thorsteinsson, T. and Berthier, E.: Ice-volume changes, bias estimation of mass-balance  
14 measurements and changes in subglacial lakes derived by lidar mapping of the surface Icelandic  
15 glaciers, *Ann. Glaciol.*, 54(63), 63–74, doi:10.3189/2013AoG63A422, 2013.
- 16 Jóhannesson, T., Sigurðsson, O., Laumann, T. and Kennett, M.: Degree-day glacier mass-  
17 balance modelling with applications to glaciers in Iceland, Norway and Greenland, *J. Glaciol.*,  
18 41(138), 345–358, 1995.
- 19 [Krimmel, R. M.: Analysis of Difference Between Direct and Geodetic Mass Balance](#)  
20 [Measurements at South Cascade Glacier, Washington, Geogr. Ann., 81 \(A\), 653-658, 1999.](#)
- 21 Kääb, A.: Remote Sensing of Mountain Glaciers and Permafrost Creep, Geographisches Institut  
22 der Universität Zürich, Zürich, 2005.
- 23 Kraus, K.: Photogrammetry – Geometry from Images and Laser Scans., 2nd edition; de Gruyter:  
24 Vienna, Austria, 2007.
- 25 Kunz, M., Mills, J.P., Miller, P.E., King, M.A., Fox, A.J., Marsh, S.: Application of surface  
26 matching for improved measurements of historic glacier volume change in the Antarctic  
27 Peninsula. *Int. Arch. Photogramm. Remote Sens. Spatial Inform. Sci.*, 39 (8), 579–584, 2012.
- 28 Lee, S.-Y., Carle, S. F. and Fogg, G. E.: Geologic heterogeneity and a comparison of two  
29 geostatistical models; sequential Gaussian and transition probability-based geostatistical  
30 simulation, *Adv. Water Resour.*, 30(9), 1914–1932, doi:10.1016/j.advwatres.2007.03.005,  
31 2007.

- 1 Nuth, C. and Kääb, A.: Co-registration and bias corrections of satellite elevation data sets for  
2 quantifying glacier thickness change, *The Cryosphere*, 5(1), 271–290, doi:10.5194/tc-5-271-  
3 2011, 2011.
- 4 Nuth, C., Kohler, J., Aas, H. F., Brandt, O. and Hagen, J. O.: Glacier geometry and elevation  
5 changes on Svalbard (1936-90); a baseline dataset, *Ann. Glaciol.*, 46, 106–116,  
6 doi:10.3189/172756407782871440, 2007.
- 7 Pálsson, F., Guðmundsson, S., Björnsson, H., Berthier, E., Magnússon, E., Guðmundsson, S.  
8 and Haraldsson, H.: Mass and volume changes of Langjökull ice cap, Iceland, ~1890 to 2009,  
9 deduced from old maps, satellite images and in situ mass balance measurements. *Jökull*, 62:  
10 81-96, 2012.
- 11 [Papasodoro, C., Berthier, E., Royer, A., Zdanowicz, C. and Langlois, A.: Area, elevation and](#)  
12 [mass changes of the two southernmost ice caps of the Canadian Arctic Archipelago between](#)  
13 [1952 and 2014, \*The Cryosphere\*, 9\(4\), 1535–1550, doi:10.5194/tc-9-1535-2015, 2015.](#)
- 14 Rolstad, C., Haug, T. and Denby, B.: Spatially integrated geodetic glacier mass balance and its  
15 uncertainty based on geostatistical analysis; application to the western Svartisen ice cap,  
16 Norway, *J. Glaciol.*, 55(192), 666–680, 2009.
- 17 ~~Rögnvaldsson, Ó., Ágústsson, H. and Ólafsson, H.: Aflræn niðurkvörðun veðurs innan LOKS~~  
18 ~~verkefnisins (Dynamical downscaling of weather within the LOKS project). Tech. Rep.,~~  
19 ~~Reiknistofa í veðurfræði, 29 pp, 2011.~~
- 20 Rusu, R. B. and Cousins, S.: 3D is here: Point Cloud Library (PCL), IEEE, 2011.
- 21 [Soruco, A., Vincent, C., Francou, B. and Gonzalez, J. F.: Glacier decline between 1963 and](#)  
22 [2006 in the Cordillera Real, Bolivia, \*Geophysical Research Letters\*, 36\(L03502\),](#)  
23 [doi:10.1029/2008GL036238, 2009.](#)
- 24 ~~Skamarock, W. C., Klemp, J. B., Dudhia, J., Gill, D. O., Barker, D. M., Duda, M. G., Huang,~~  
25 ~~X. Y., Wang, W. and Powers, J. G.: A description of the Advanced Research WRF version 3.~~  
26 ~~Technical Report NCAR/TN-475+STR, National center for atmospheric research, 2008.~~
- 27 Spriggs, R. M.: The calibration of Military Cartographic Cameras, Technical Note, Intelligence  
28 and Mapping R. & D. Agency., 1966.
- 29 Thibert, E., Blanc, R., Vincent, C. and Eckert, N.: Instruments and methods; glaciological and  
30 volumetric mass-balance measurements; error analysis over 51 years for Glacier de Sarennes,  
31 French Alps, *J. Glaciol.*, 54(186), 522–532, doi:10.3189/002214308785837093, 2008.

1 Trüssel, B. L., Motyka, R. J., Truffer, M. and Larsen, C. F.: Rapid thinning of lake-calving  
2 Yakutat Glacier and the collapse of the Yakutat Icefield, southeast Alaska, USA, *J. Glaciol.*,  
3 59(213), 149–161, 2013.

4 Uppala, S. M., Kallberg, P. W., Simmons, A. J., Andrae, U., Da Costa Bechtold, V., Fiorino,  
5 M., Gibson, J. K., Haseler, J., Hernandez, A., Kelly, G. A., Li, X., Onogi, K., Saarinen, S.,  
6 Sokka, N., Allan, R. P., Andersson, E., Arpe, K., Balmaseda, M. A., Beljaars, A. C. M., Van  
7 De Berg, L., Bidlot, J., Bormann, N., Caires, S., Chevallier, F., Dethof, A., Dragosavac, M.,  
8 Fuentes, M., Hagemann, S., Holm, E., Hoskins, B. J., Isaksen, L., Janssen, P. A. E. M., Jenne,  
9 R., McNally, A. P., Mahfouf, J. F., Morcrette, J. J., Rayner, N. A., Saunders, R. W., Simon, P.,  
10 Sterl, A., Trenberth, K. E., Untch, A., Vasiljevic, D., Viterbo, P. and Woollen, J.: The ERA-40  
11 re-analysis, *Q. J. R. Meteorol. Soc.*, 131(612), 2961–3012, 2005.

12 Vaughan, D. G., Comiso, J. C. and I. Allison, J. Carrasco, G. Kaser, R. Kwok, P. Mote, T.  
13 Murray, F. Paul, J. Ren, E. Rignot, O. Solomina, K. Steffen and T. Zhang: Observations:  
14 Cryosphere, in *Climate Change 2013: The Physical Science Basis. Contribution of Working*  
15 *Group I to the Fifth Assessment Report of the Intergovernmental Panel on Climate Change*,  
16 edited by Stocker T.F., D. Qin, G.-K. Plattner, M. Tignor, S.K. Allen, J. Boschung, A. Nauels,  
17 Y. Xia, V. Bex and P.M. Midgley, pp. 317–382, Cambridge University Press, Cambridge,  
18 United Kingdom and New York, NY, USA., 2013.

19 Wolf, P. and Dewitt, B. A.: *Elements of photogrammetry; with applications in GIS*, McCraw  
20 Hill : Boston, MA, United States, United States, 2000.

21 Zemp, M., Thibert, E., Huss, M., Stumm, D., Rolstad Denby, C., Nuth, C., Nussbaumer, S. U.,  
22 Moholdt, G., Mercer, A., Mayer, C., Joerg, P. C., Jansson, P., Hynek, B., Fischer, A., Escher-  
23 Vetter, H., Elvehøy, H. and Andreassen, L. M.: Reanalysing glacier mass balance measurement  
24 series, *The Cryosphere*, 7(4), 1227–1245, doi:10.5194/tc-7-1227-2013, 2013.

25

1 Table 1. Dates, main parameters and notes describing the data sets used in the study. \*GSD:  
 2 Ground Sampling Distance.

3

Date	N. Images	Average GSD* (m)	Notes
12.10.1946	15	0.94	Missing southernmost part of Drangajökull. Over-exposed areas
Summer 1960	40	0.42	Divided in 3 flights: 14.06.1960, 08.07.1960 and 12.7.1960.
05.09.1975	18	0.77	Missing Leirufjarðarjökull outlet.
27.07.1985	32	0.70	Missing Reykjarfjarðarjökull outlet.
04.08.1986	5	0.70	Used for filling the gaps of 1985 on Reykjarfjarðarjökull outlet
29.08.1994	21	0.53	Missing southern part
27.07.2005	57	0.53	Complete coverage
20.07.2011	-	-	Complete coverage (LiDAR)

4

1 Table 2. The horizontal RMSE of the GCPs (nr. of GCPs within brackets), glacier coverage and  
 2 error assessment of the photogrammetric DEMs, using four different approaches: i) Direct  
 3 comparisons of ice-free areas (mean and standard deviation). ii) Comparisons in ice-free areas  
 4 after masking out outliers and areas with slope > 20° (see Sect. 2.2). iii) SGSim.  $z\_bias$   
 5 corresponds the mean elevation bias from 1000 simulation,  $z\_bias_u$  and  $z\_bias_l$  the upper and  
 6 lower 95% confidence level and  $\Delta z\_bias = (z\_bias_u - z\_bias_l)/2$ . iv) Method described by Rolstad  
 7 et al., (2009). To derive uncertainties with 95% conf. level we assume normal probability  
 8 function and therefore  $\Delta z\_bias_{Rols.} = 1.96 * \sigma_{z\_bias\_Rols.}$

9

Year	RMSE XY GCPs (m)	Glacier cover- age (%)	Error mean ice- free (m)	Std. dev. ice-free (m)	Error mean ice-free masked (m)	Std. dev. ice-free masked (m)	$z\_bias$ (m)	$z\_bias_l$ (m)	$z\_bias_u$ (m)	$\Delta z\_bias$ (m)	$\Delta z\_bias$ Rols. (m)
1946	2.99 [43]	75.3	-0.95	5.09	-0.86	4.80	1.66	0.12	3.27	1.58	3.41
1960 W	2.87 [25]	31.0	0.37	2.23	0.49	1.84	0.48	-0.34	1.34	0.84	1.05
1960 C	2.54 [31]	30.5	-0.31	2.08	-0.26	1.52	0.34	-0.29	1.02	0.66	1.04
1960 E	2.21 [47]	35.6	0.03	2.26	0.09	1.51	0.20	-0.45	0.93	0.69	0.96
1975	1.22 [44]	96.5	0.48	2.05	0.39	1.52	0.03	-0.47	0.48	0.48	0.62
1985	1.37 [33]	87.2	-0.67	1.97	-0.60	1.15	-0.48	-0.80	-0.17	0.32	0.47
1994	0.84 [40]	66.3	-0.09	1.04	-0.09	0.80	0.22	-0.03	0.47	0.25	0.72
2005	1.14 [55]	100.0	-0.24	1.30	-0.26	0.87	0.22	0.01	0.42	0.21	0.78

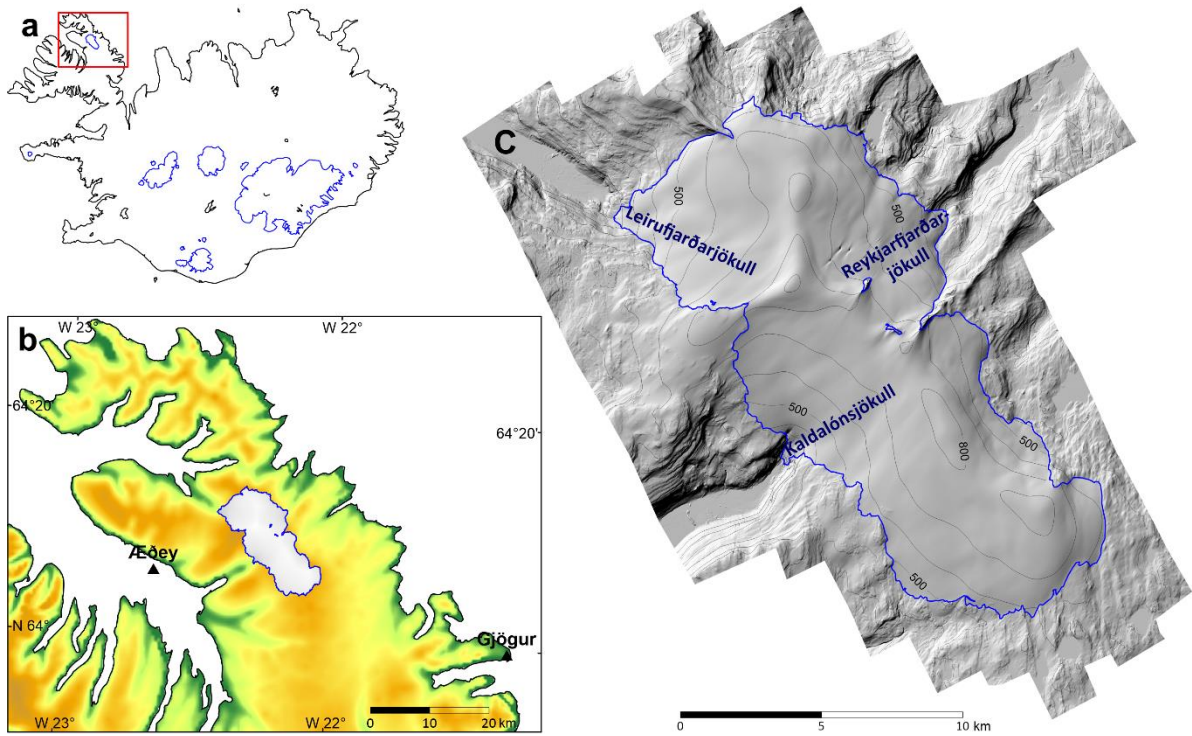
10

1 Table 3. The average elevation change during periods defined by the DEMs before ( $\delta h$ ) and  
 2 after ( $\delta h^*$ ) the seasonal correction, the seasonal correction ( $\delta h_{S\_cor}$ ) corresponding to DEM at  
 3 time  $t_s$  and  $t_f$  (the correction at  $t_f$  is shown with minus sign since this correction term has minus  
 4 in front of it in Eq. 2), the uncertainties (95% conf. level) of seasonally corrected elevation  
 5 change ( $\Delta\delta h^*$ ) and the uncertainty contribution from the seasonal corrections ( $\Delta\delta h_{S\_cor}$ ), DEM  
 6 errors ( $\Delta\delta h_m$ ) and interpolation of data gaps ( $\Delta\delta h_i$ ), respectively. All values were originally  
 7 calculated in terms of volumes but are here averaged over the area  $\bar{A}=(A(t_f)+ A(t_s))/2$ .

8

$t_s$	$t_f$	Average $\delta h$ (m)	Average $\delta h^*$ (m)	Average $\delta h_{S\_cor}(t_s)$ (m)	Average $-\delta h_{S\_cor}(t_f)$ (m)	Average $\Delta\delta h^*$ (m)	Average $\Delta\delta h_{S\_cor}$ (m)	Average $\Delta\delta h_m$ (m)	Average $\Delta\delta h_i$ (m)
1946	1960	-7.36	- 10.3489	0	-23.5395	2.734	10.909	1.28	2.19
1960	1975	-4.73	-1.8427	3.0869	-0.1822	1.3329	1.0314	0.62	0.39
1975	1985	2.06	1.0608 6	0.1922	-1.1842	0.9695	0.404	0.54	0.62
1985	1994	2.15	2.8473	1.1942	-0.6174	1.1514	0.4944	0.32	1.08
1994	2005	-7.11	-8.209	0.6274	-1.6092	1.17	0.6358	0.26	0.96
2005	2011	-2.38	-32.283	1.6294	-2.0779	0.99100	0.9795	0.21	0

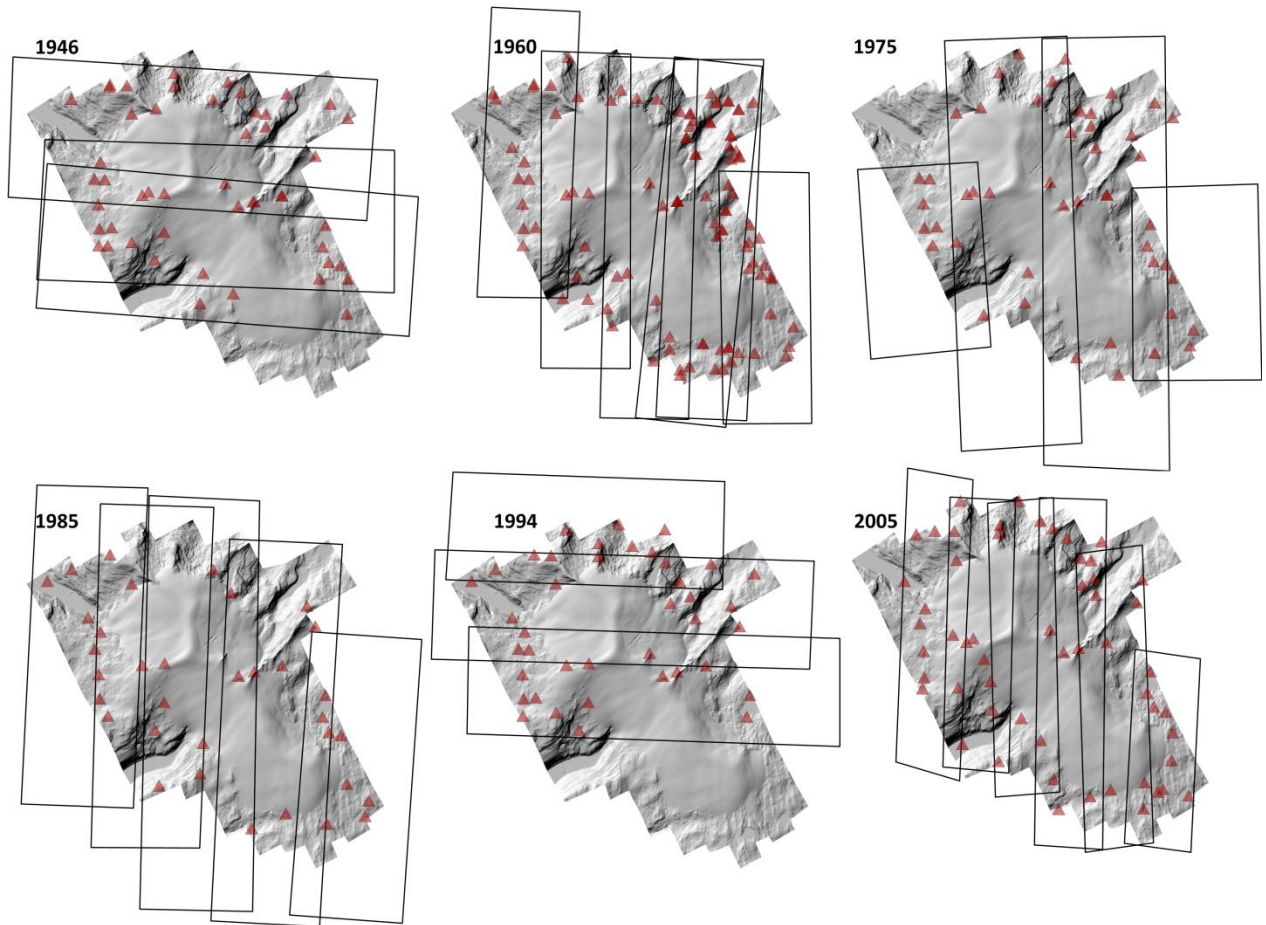
9



1

2

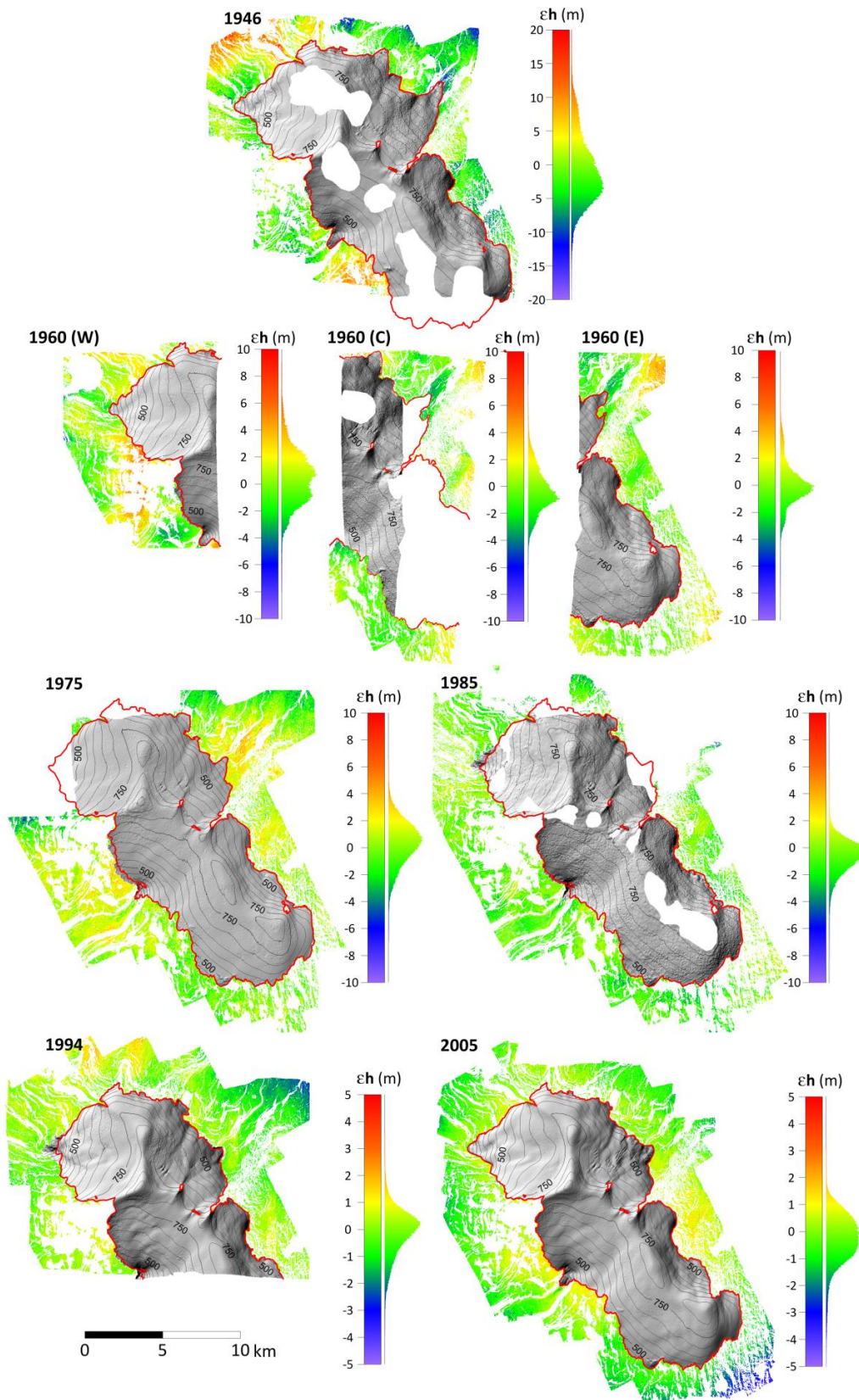
3 Figure 1. Location of study area. Blue lines in **a** are the outline of the larger glaciated areas in  
 4 Iceland ~~and the letters L and V indicates the location of Langjökull and Vatnajökull ice caps,~~  
 5 ~~respectively~~. The triangles in **b** indicates the locations of the meteorological stations at Aðey  
 6 and Gjögur. Image **c** shows a Lidar DEM of Drangajökull (glacier margin shown with blue line)  
 7 and vicinity obtained in 2011 (Jóhannesson et al., 2013) represented as shaded relief image and  
 8 contour map (100 m contour interval). The names and locations of the 3 main outlet glaciers  
 9 are shown.



1

2

3 Figure 2. The coverage of aerial photographs at different epochs with the LiDAR DEM as  
4 background. The GCPs used for orientation of each series of aerial photographs are marked  
5 with triangles.

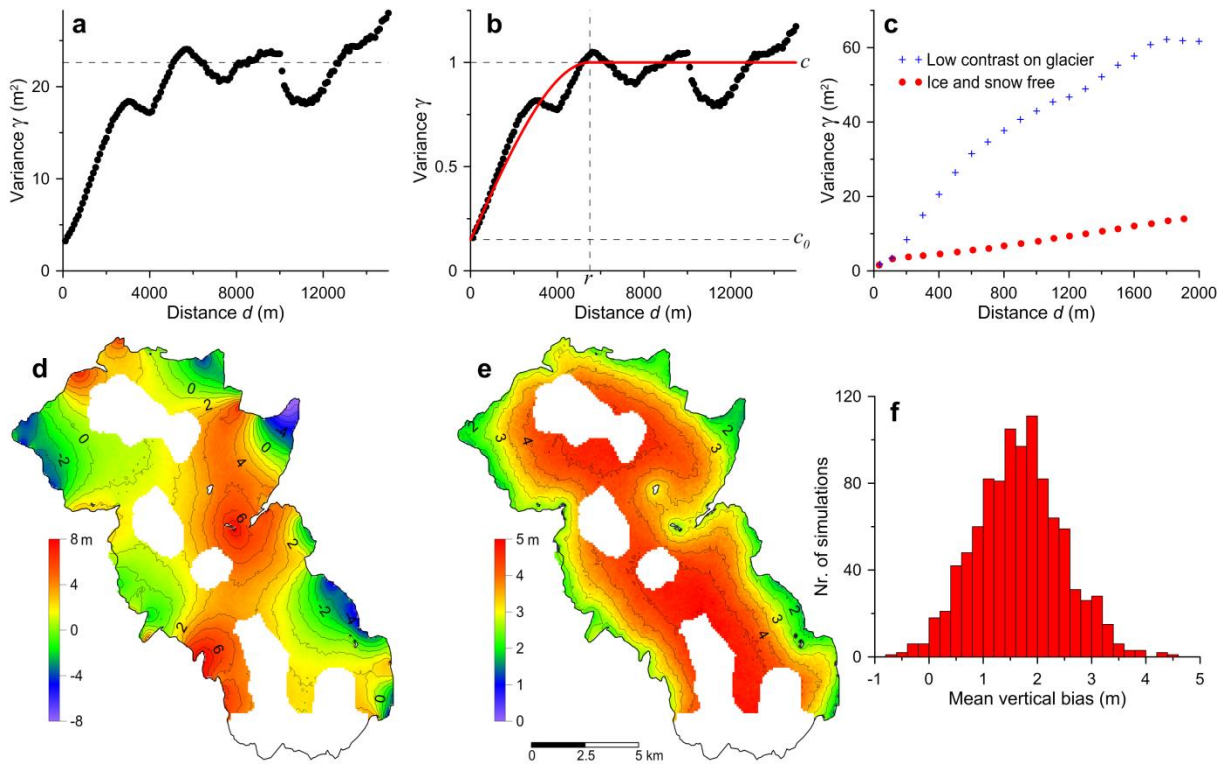


1

2

1 Figure 3. The series of DEMs of Drangajökull ice cap created from the aerial photographs. The  
 2 shaded relief images and contour maps indicate the glaciated part of each DEM. The elevation  
 3 differencederived elevation errors in the vicinity of the glacier off ice (after masking out outliers  
 4 and areas with slope >20°) are shown as color images. The color scale is extended for the DEM  
 5 in 1946 and reduced for the 1994 and 2005 DEMs. A vertical histogram next to the scale bar  
 6 shows the error distribution.

7

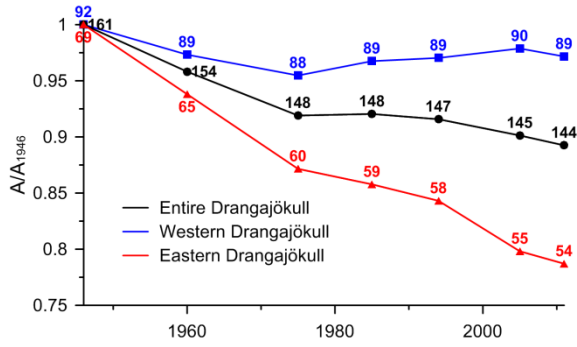


8

9

10 Figure 4. The semivariograms of the 1946 DEM error before (a) and after (b) nscoring the data.  
 11 The DEM error data is derived from the elevation difference compared to the LiDAR DEM in  
 12 ice and snow free areas. Outliers in the elevation difference and areas with slope >20° were also  
 13 masked out. The spherical semivariogram model (red line) used in the SGSim and the  
 14 parameters defining it ( $c$ ,  $c_0$  and  $r$ ) are shown in b. Graph c shows comparison between  
 15 semivariograms for the deduced error (same as in a) and the difference compared to the LiDAR  
 16 DEM in low contrast areas within the glacier. d-f shows the results of the SGSim for the 1946  
 17 glacier DEM. Images d and e, respectively show the mean and standard deviation of 1000  
 18 simulations at each 100mx100m pixel. Graph f shows histogram (0.2 m bins) of the mean  
 19 vertical bias values of the glacier DEM deduced from each simulation.

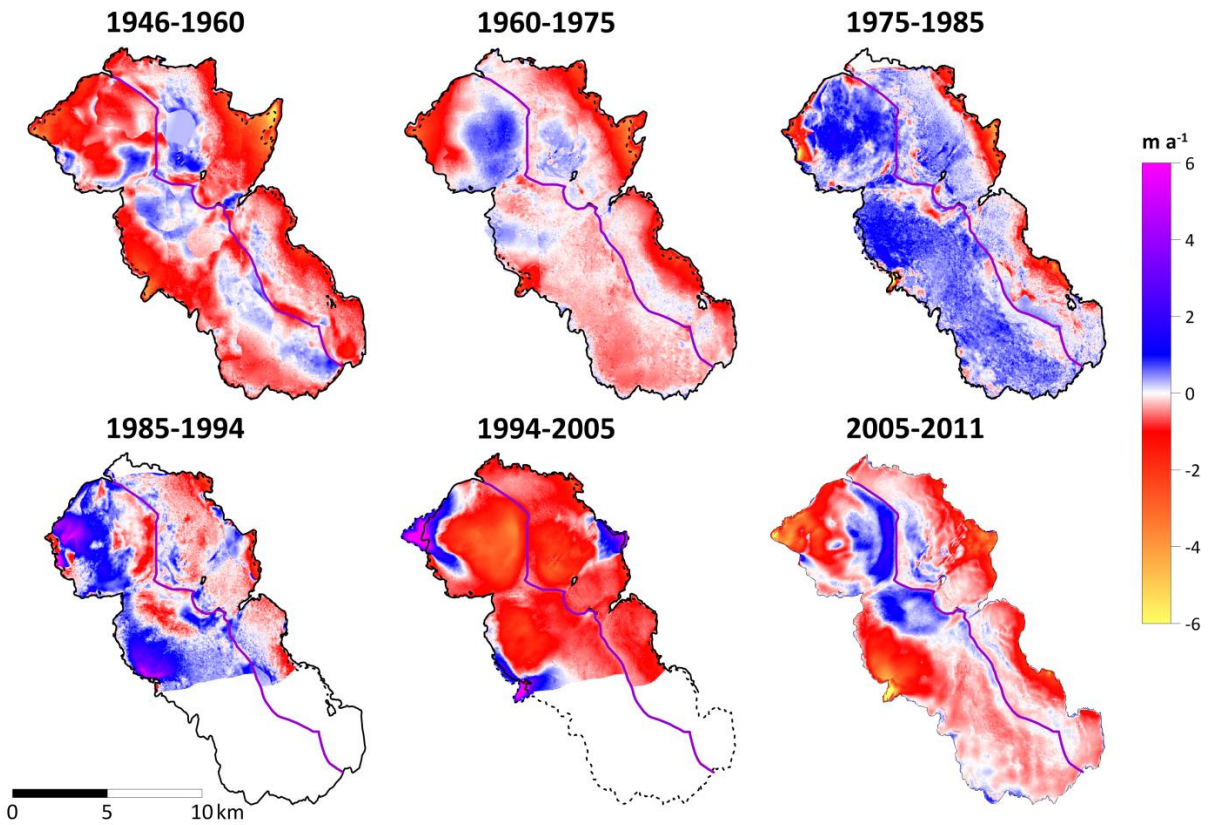
1



2

3

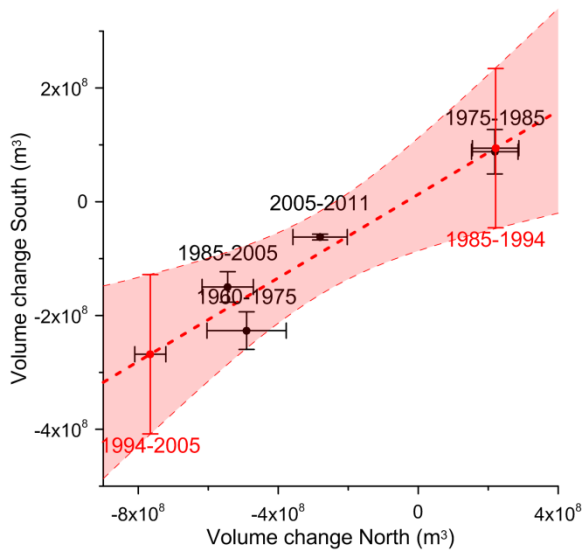
4 Figure 5. The relative area change of all, the western and the eastern sections of Drangajökull  
 5 ice cap (relative to the initial area in 1946). The purple lines in Fig. 6 show the ice divides; they  
 6 are used to define the east and west sections of the glacier. Labels give the glacier area in km<sup>2</sup>  
 7 at each epoch.



8

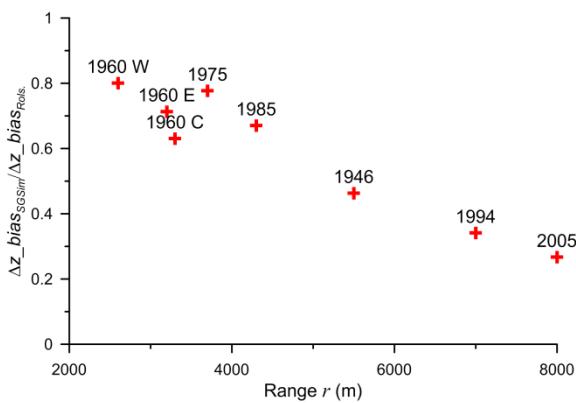
9

10 Figure 6. The average annual elevation change of Drangajökull during 6 intervals since 1946.  
 11 Red colors indicate thinning and blue colors thickening.



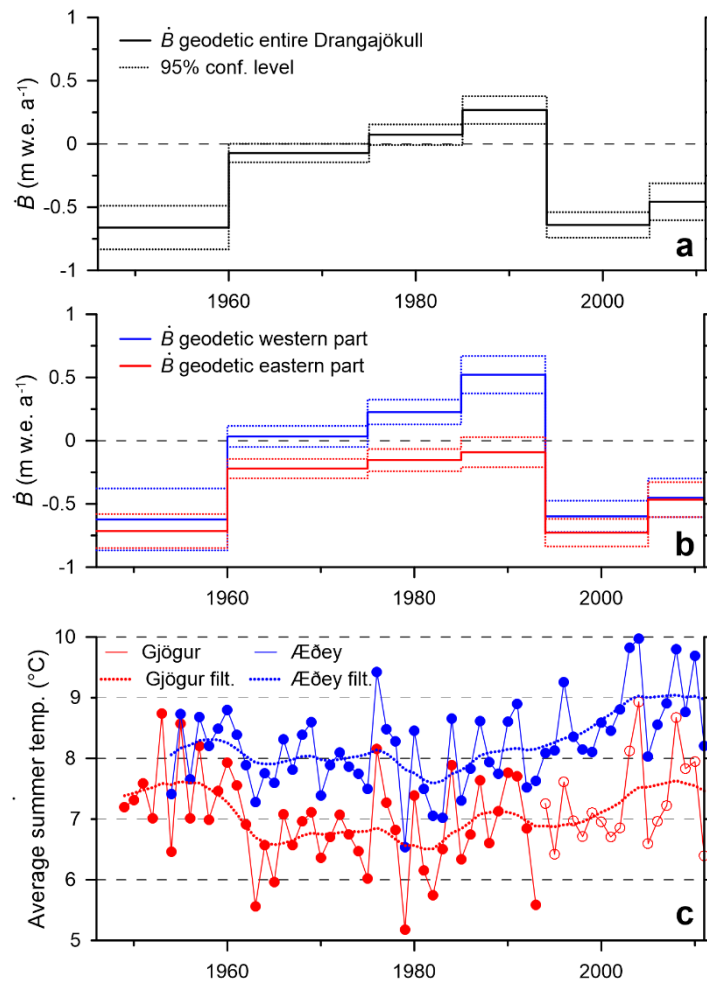
1  
2  
3  
4  
5  
6  
7  
8

Figure 7. The volume change of the southernmost of Drangajökull, which is missing in the 1994 DEM (Fig. 3), plotted as function of the volume change in the area north of it covered by the 1994 DEM, for the periods available (shown with black labels). The thick dashed line shows linear fit for the data points with the 95% confidence area shown as light red. The red dots are the corresponding volume change estimates for the southern part in 1985-1994 and 1994-2005.



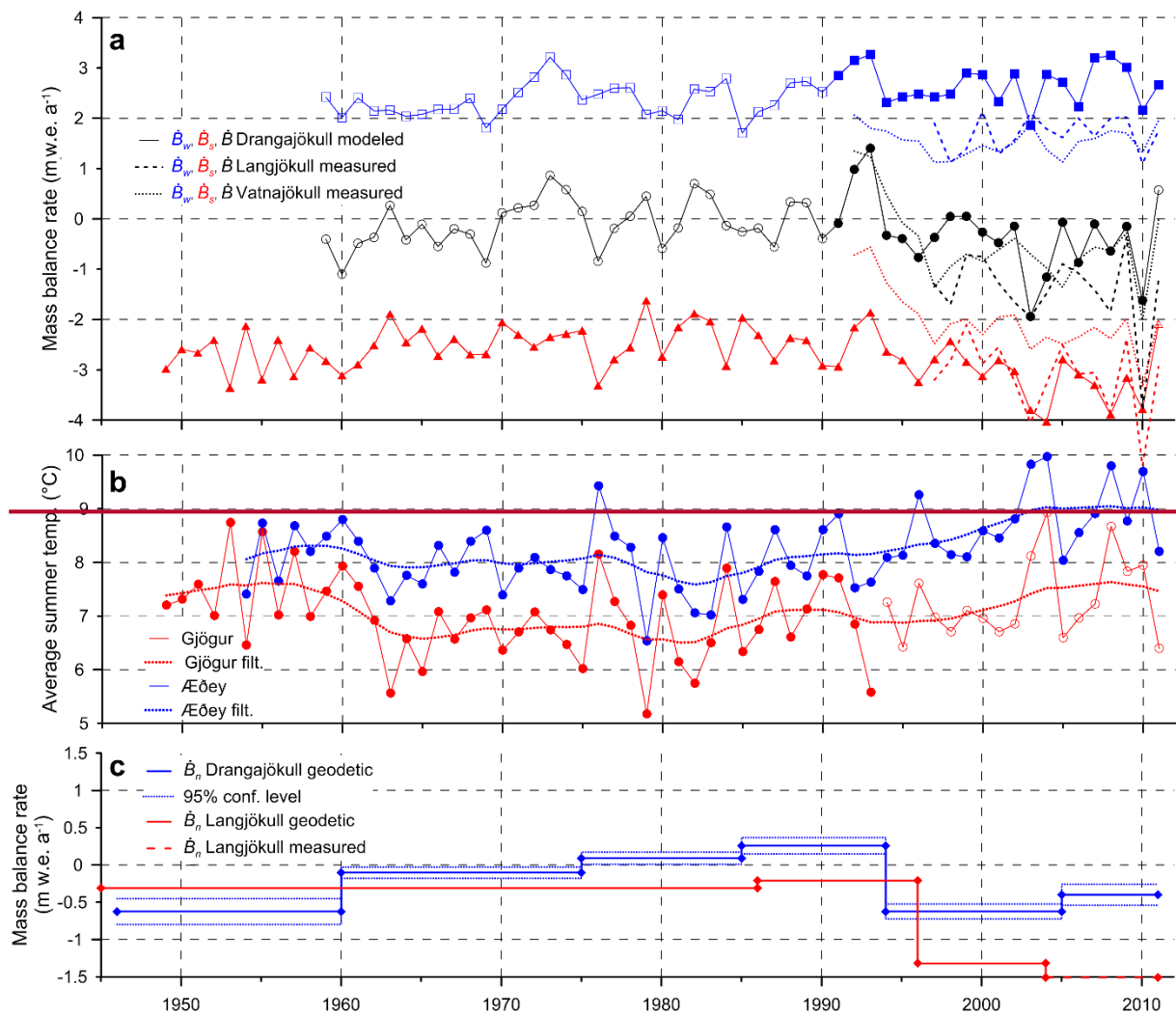
9  
10  
11  
12  
13  
14  
15

Figure 8. The ratio between uncertainties (95% conf. level) from the methods demonstrated in this work and the method demonstrated by Rolstad et al. (2009) as function of the range,  $r$ , in the deduced spherical semivariogram model. The DEM epoch corresponding to each point is shown with a label.



1  
2

3 Figure 9. The glacier-wide mass balance rate ( $\dot{B}$ ) during 6 different periods since 1946,  
 4 calculated for the entire ice cap (a) of all, as well as when and split into the western and the  
 5 eastern sections of Drangajökull (b) using the ice divides shown asThe purple lines in Fig. 6.  
 6 show the ice divides used to splitting the ice cap between the east and west sections.The dotted  
 7 line in a-b represent 95% confidence level. Graph c shows the average summer temperature at  
 8 the meteorological stations Gjögur, since 1949, and Æðey since 1954 (see Fig. 1b, for  
 9 locations). Close circles indicate data from manned station, open circles from automatic station.  
 10 The dotted lines show the average summer temperature at each location filtered with 11 year  
 11 triangular fiweighted kerrunning average. ice cap during 6 different periods since 1946, derived  
 12 with geodetic methods (blue line). The purple lines in Fig. 6 show the ice divides used to  
 13 splitting the ice cap between the east and west sections. The dashed red line shows the glacier-  
 14 wide mass balance rate for the same periods estimated from mass balance model (see Sect. 2.6  
 15 and Fig. 10).



1

2

3 **Figure 10. a)** The modeled glacier wide mass balance rate (summer, winter and net) of  
 4 Drangajökull (solid lines). Closed blue boxes denote annual values  $\hat{B}_w$  derived by integrating  
 5 in space and during given winter daily precipitation maps interpolated from bias corrected rain-  
 6 gauge measurements (Crochet, 2013). Open blue boxes, denotes  $\hat{B}_w$  derived using daily  
 7 precipitation maps downscaled from ERA 40 (an update of Crochet et al. (2007) described in  
 8 Jóhannesson et al. (2007)), multiplied with a scaling factor (see Sect. 2.6). The closed red  
 9 triangles show  $B_s$  derived with degree day model using the daily grids of interpolated  
 10 temperature at 2 m height above ground (Crochet and Jóhannesson, 2011) available in 1949–  
 11 2010. The open triangle in 2011 is derived using temperature at 2 m height from Rögnvaldsson  
 12 et al., (2011) and *ddf* scaled for the period 2005–2011 (see Sect. 2.6). The dash and dot line  
 13 shows for comparison measured values of  $\hat{B}_w, \hat{B}_s$  and  $\hat{B}$  for Langjökull and Vatnajökull ice  
 14 caps, respectively (Björnsson et al., 1998; 2013). **b)** The average summer temperature at the

1 meteorological stations Gjögur, since 1949, and Æðey since 1954 (see Fig. 1b, for locations).  
2 Close circles indicate data from manned station, open circles from automatic station. The dot  
3 lines show the average summer temperature at each location filtered with 11 year triangular  
4 filter. e) The geodetic results of  $\dot{B}$  for Drangajökull ice cap, compared with geodetic  
5 observations from Langjökull ice cap (Pálsson et al., 2012). The record is extended to 2011 for  
6 Langjökull with traditional mass balance measurements shown in a. See Fig. 1a for locations.